

**SKB P-22-27**

ISSN 1651-4416

ID 1982333

November 2024

# Geometry and mechanical properties of water bearing fractures

Eva Hakami, Sofia Winell  
Rejlers AB

Abel Sánchez Juncal  
Svensk Kärnbränslehantering AB

*Keywords:* Fracture characterization, Fracture surface, Fracture mineralogy, Posiva Flow Log, PFL, Leeb hardness test, Hardness, Aperture, Acoustic televiewer

Data in SKB's database can be changed for different reasons. Minor changes in SKB's database will not necessarily result in a revised report. Data revisions may also be presented as supplements, available at [www.skb.se](http://www.skb.se).

This report is published on [www.skb.se](http://www.skb.se)

© 2024 Svensk Kärnbränslehantering AB

## Abstract

As a part of the site investigations at Forsmark, the transmissivity along boreholes has previously been measured with the Posiva Flow Log (PFL) method, and the depth of the fractures corresponding to the more transmissive sections has been identified. The aim of this study was to investigate whether the mechanical properties of these "PFL-fractures" differ from the properties of other open fractures. With this objective, a system for classification of geometrical characteristics of PFL-fractures was proposed, and acoustic televiewer images were utilized to perform these studies. Core mapping (Boremap) data were used to compare mapped fracture surface parameters of the group of PFL-fractures with the group of all open fractures. Further, the Leeb hardness test method (LHT) was for the first time introduced and tested on Forsmark samples, both on sawn intact rock surfaces and on different types of natural fracture surfaces.

About 65 % of the PFL-anomalies (short sections with transmissivity  $> 10^{-9} \text{ m}^2/\text{s}$ ) were found to be correlated to a single open fracture, and about 35 % to a more complex geometry structure, such as several close fractures. There is on average a correlation between the fracture geometrical classes defined and the measured transmissivity, even if the spread is large. No major difference was found between PFL-fractures and Non-PFL fractures with regard to the core mapping parameters, with the exception of the "Aperture". The LHT indicated that the single PFL-fractures should be expected to have softer fracture surfaces compared to the Non-PFL fractures. The particular LHT instrument used in this study was, however, found to have some limitations in its application both on intact rock surfaces and natural rock fracture surfaces with mineral coatings.

## Sammanfattning

Inom ramen för platsundersökningarna i Forsmark har transmissiviteten längs borrhål tidigare uppmätts med Posiva Flow Log, och djupet till de sprickor som korrelerar med sektioner med större transmissivitet har på detta sätt identifierats. Syftet med denna studie är att undersöka om dessa "PFL-sprickor" har mekaniska egenskaper som skiljer sig från egenskaperna hos andra öppna sprickor. Med det syftet föreslås ett system för att klassificera de olika geometriska kategorierna hos PFL-sprickorna och bilder från akustisk televiewer användes för att studera detta. Data från kärnkartering med Boremap användes för att jämföra karterade sprickytparametrar hos gruppen PFL-sprickor respektive gruppen samtliga öppna sprickor. Dessutom testades Leeb hårdhetsmätare (LHT) för första gången, både på sågade ytor av intakt berg och på olika naturliga sprickytor.

Omkring 65 % av PFL-anomalierna (korta sektioner med transmissivitet  $> 10^{-9} \text{ m}^2/\text{s}$ ) var korrelerade till enskilda öppna sprickor, och omkring 35 % till mera komplexa geometriska strukturer, såsom flera näraliggande sprickor. Det finns generellt ett samband mellan sprickornas geometriska uttryck i borrhålsväggen och dess transmissivitet, även om spridningen är stor. Ingen väsentlig skillnad kunde observeras mellan PFL-sprickor och andra sprickor, vad gäller kärnkarteringsparametrar, med undantag för parametern "Apertur". LHT indikerade att PFL-sprickorna kan i medeltal förväntas ha mjukare sprickytor jämfört med icke-PFL-sprickor. Det specifika LHT-instrumentet som använts hade dock vissa begränsningar i sin tillämpning, både på släta ytor av intakt berg och på naturliga sprickytor med sprickfyllnadsmineral.

# Content

<b>1</b>	<b>Introduction</b> .....	<b>3</b>
1.1	Background .....	3
1.2	Objective and scope.....	3
<b>2</b>	<b>Geometrical study of PFL-fractures in borehole images</b> .....	<b>4</b>
2.1	Analysis using acoustic televiewer logs .....	4
2.1.1	Included boreholes .....	4
2.1.2	Geometrical classes .....	4
2.2	Geometry class distribution in ten KFM boreholes.....	6
2.3	Correlations between geometry class and transmissivity.....	9
<b>3</b>	<b>Comparison of Boremap parameters for PFL-fractures and the other open fractures</b> .....	<b>11</b>
3.1	Data set included in study .....	11
3.2	Surface and roughness.....	12
3.3	Joint alteration and $J_a$ .....	13
3.4	Fracture aperture .....	14
3.5	Fracture mineral .....	16
<b>4</b>	<b>Surface matedness of PFL-fractures</b> .....	<b>18</b>
4.1	Matedness – Aperture spatial correlation .....	18
4.2	Aperture measurement using viscous silicon .....	21
<b>5</b>	<b>Surface hardness studies using Leeb Hardness Test (LHT)</b> .....	<b>22</b>
5.1	Instrument and methodology.....	22
5.2	LHT on intact rock surfaces from Forsmark .....	23
5.2.1	Complementary Leeb hardness tests and comparison with UCS and ITS for amphibolite .....	29
5.3	LHT on PFL-fracture surfaces .....	33
5.4	LHT on natural Non-PFL-fracture surfaces .....	35
5.5	Comparison of LHT on PFL-fractures and Non-PFL-fracture surfaces.....	37
5.6	Correlation between LHT and detailed infilling mapping.....	38
5.7	Complementary LHT with different hardness scales .....	38
5.8	Discussion on Leeb hardness test (LHT) device and method.....	40
<b>6</b>	<b>Summarizing conclusions and recommendations</b> .....	<b>41</b>
6.1	Comparison between PFL-fractures and Non-PFL-fractures .....	41
6.2	Recommendations and concluding remarks .....	42
	<b>References</b> .....	<b>43</b>
	<b>Appendix A – Acoustic televiewer image files with geometry classification of PFL anomalies</b> .....	<b>45</b>
	<b>Appendix B – Photographs of studied PFL-fracture surfaces</b> .....	<b>49</b>

# 1 Introduction

## 1.1 Background

The water bearing fractures are one of the main components in the safety assessment of a spent nuclear fuel storage. The properties of water bearing fractures in the rock mass are important in the assessment of containment and radionuclide retardation. The mechanical properties of fractures are one of the fundamental factors involved in such analysis, in particular when they are considered stress dependent and used in hydro-mechanical coupled models, as described in the methodology for rock mechanics modelling (Hakami et al. 2022). In discrete fracture network (DFN) models the properties of the fractures, and their size-dependency, is one of the required inputs. The methodology for DFN-modelling is thoroughly presented in Selroos et al. (2022).

Within the site investigations performed at the Forsmark Site, borehole hydraulic testing has been a major activity. To identify the significant water bearing fractures, among all the natural fractures existing in the rock mass, measurements with the Posiva Flow Log (PFL) method have been performed. The result from this logging is the location of sections, so called PFL anomalies, where the flow is higher than a particular measurement limit. These results, in combination with borehole optical logging and core mapping have thereafter been used to correlate the PFL anomalies with certain single fractures (Forsman et al. 2004, 2006, 2008). These fractures that have been identified as the main contributors to the water inflow, in the corresponding borehole section, are in this report hereafter called “PFL-fractures”.

The size of PFL-fractures is of course not directly measurable, since they are only observed in boreholes, but, according to Selroos et al. (2022), there is a general expectation that a correlation exists between fractures size and fracture transmissivity. This means that it is of interest to study whether the larger fractures, or the PFL-fractures, would present different characteristics compared to the fractures that are not PFL-fractures (these much more frequently occurring “ordinary” open fractures are hereafter called “Non-PFL-fractures”). Furthermore, any difference in aperture distribution, and transmissivity, suggests that the mechanical properties, such as stiffness and strength, potentially also differ between the PFL-fractures and the Non-PFL-fractures. In previous site descriptions, however, no specific parameter estimation was attempted for the water bearing fractures (Glamheden et al. 2007).

This is the background to why investigations allowing for better estimates of the PFL-fracture mechanical properties are recommended in the updated methodology for rock mechanics modelling (Hakami et al. 2022), and it is the motivation for the study in the present report.

## 1.2 Objective and scope

The objective of this study is to investigate potential differences between PFL-fractures and Non-PFL-fractures in Forsmark, with respect to the relevant parameters for their mechanical characterization. The scope includes the analysis of the existing database (desktop study, presented in Chapter 2) and, for a selected number of fractures, studies on existing drill cores from the site (Chapter 3 and 4). This study is a pilot investigation in which previously not applied techniques, mainly the Leeb hardness test, have been evaluated for their potential use in subsequent studies.

## 2 Geometrical study of PFL-fractures in borehole images

### 2.1 Analysis using acoustic televiewer logs

To be able to properly describe the water bearing fractures, i.e. the aforementioned PFL-fractures, a better understanding of their geometrical features is needed. Previous studies on borehole breakouts using acoustic televiewer (AT) boreholes loggings suggested the idea that this log could be used as an appropriate tool for improving the characterization of these PFL-fractures. Softer, hollow, deeper or irregular points at the drilled borehole wall will turn out as darker points in the AT-log amplitude presentation images. The principles of the televiewer tool are explained in Ringgaard (2007). The acoustic televiewer log has been used in many, but not all, of the core drilled boreholes in Forsmark.

#### 2.1.1 Included boreholes

The selection of boreholes to include in this study is based on available boreholes with AT-logs, the quality of these AT-log files and the existence of Posiva Flow Log (PFL) data. Boreholes logged with a horizontal quality resolution less than 120 pixels along the borehole perimeter have been excluded from the classification. The classified boreholes are presented in Table 2-1.

**Table 2-1 Boreholes included in geometrical classification of PFL-anomalies.**

Borehole ID	Length interval (m)	AT-log quality (pixels)
KFM01A	100-1000	120
KFM01D	91-787	180
KFM02A	100-1002	120
KFM02B	88-572	120
KFM04A	109-1000	No information available
KFM05A	110-1000	No information available
KFM08C	102-949	180
KFM08D	60-929	120
KFM10A	62-496	180
KFM11A	72-625	180

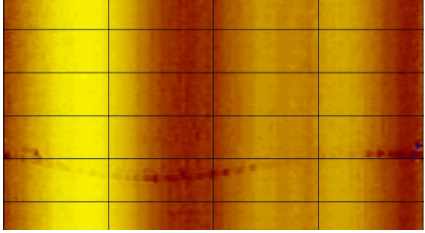
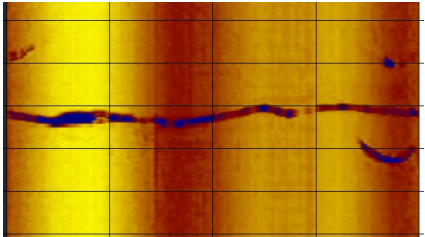
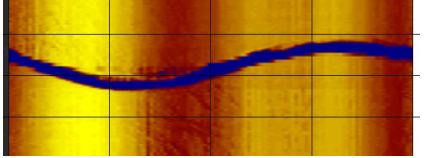
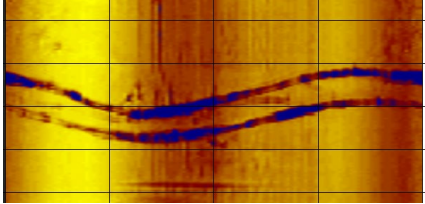
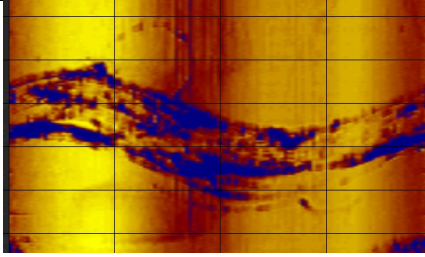
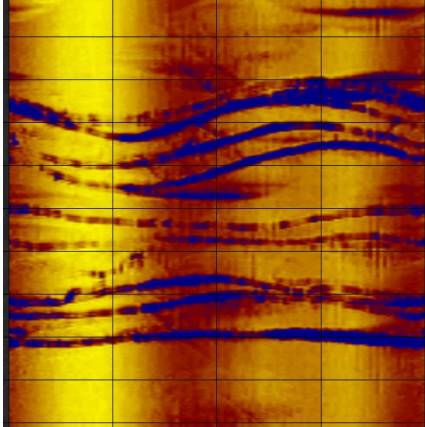
#### 2.1.2 Geometrical classes

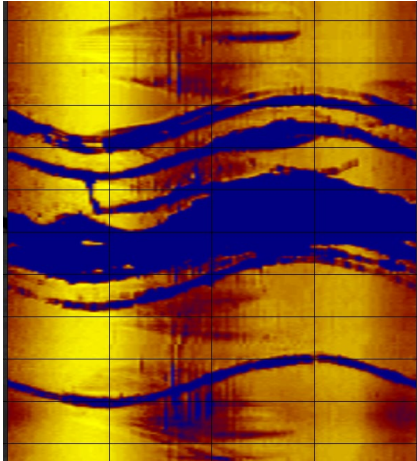
In the work by Forssman et al. (2004, 2006, 2008) and Teurneau B et al. (2008) each PFL anomaly is correlated with a single fracture in the core mapping. That is, in a section with a PFL anomaly there may be several fractures and, by looking at the BIPS-image, the fracture that was considered most probable to give the highest flow among all the fractures in the anomaly is called “best choice”. These fractures are found in the SICADA database. In this study, the AT-Log result was analysed at each borehole depth location for the “best choice”. Depending on the fracture geometry observed in the log image at the “best choice” fracture location, the PFL-fractures were assigned “geometry classes”. The different “typical” appearance of fractures in the AT-log image at a PFL-anomaly is presented in Table 2-2. In cases where there is only one single fracture close to the “best choice” depth, the geometry class will be one of the single fracture classes (Class I, II or III in Table 2-2). However, for the more complex cases with several fractures or crushes involved, separate geometric classes have been introduced with the aim to describe the geometry of the PFL anomalies more accurately (Class IV - VII in Table 2-2). Naturally, some PFL anomalies fall between the different geometrical classes proposed herein and the selection is not always straightforward.

Prior to the classification, the length of the AT-logs was adjusted with the mapping in Boremap for each borehole by using the groove millings in the borehole wall, approximately every fifty meters. This is to be able to correlate and ensure that the correct fracture is studied in the AT-log.

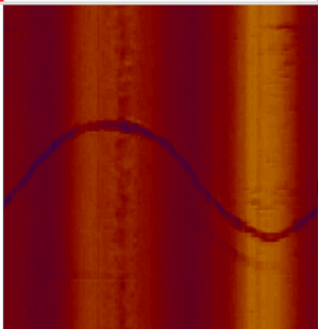
In a few cases, the “best choice” fracture according to SICADA (based on BIPS) did not seem to match with the fracture that was judged to have largest aperture at the flow anomaly in the AT-log image. In these few cases the fracture that was best correlated to the PFL anomaly according to the AT-log was used for the classification.

**Table 2-2 Description of the geometrical classes I-VII.**

Class	Description	Example
Class I	Very thin, single fracture. Clearly visible darker trace from side to side but not necessarily fully continuous along the intersection with the borehole wall.	
Class II	Clearly visible trace around the whole borehole wall. Signs of matedness between the opposing surfaces.	
Class III	Clearly visible aperture along the whole intersection with the borehole wall. No obvious signs of matedness.	
Class IV	Two or three adjacent fractures, with fracture spacing of 1-7 cm.	
Class V	A wider complex structure consisting of several fractures, crush and/or some alteration.	
Class VI	Several (> 3) parallel or crossing fractures with a separation distance of < 3 cm	

Class VII	Several parallel fractures, or a wider structure, with one dominating aperture.	
-----------	---	--

The classification is made using WellCAD as the visualizing program. The log is shown with the depth scale and an aspect ratio such that the fracture image is not distorted (x and y scale should be similar). In Appendix A all the studied AT-logs are presented, including the transmissivity from the PFL anomaly and the geometrical class for each PFL-fracture (See example in Figure 2-1). However, in the Appendix A the depth scale is strongly compressed and the WellCAD-files referred should be viewed with an appropriate aspect ratio for allowing the study of their geometry in the acoustic televiewer column.

Adjusted 1m:5m	Acoustic Televiewer 0° 90° 180° 270° 0°	Transmissivity (m2/s) 2e-10 2e-05	PFL geometry class	Comment
332.7 332.8 332.9			●	

*Figure 2-1. The results of the PFL-fracture geometry classification are stored in WellCAD of this format. See also Appendix A*

## 2.2 Geometry class distribution in ten KFM boreholes

The result from the geometry classification, as presented in Section 2.1, is presented in Table 2-3, Figure 2-2 and Figure 2-3. There are differences between the different boreholes but they are not very large. It is believed that the relative increase of Class I PFL-fractures in boreholes KFM8C, KFM10A and KFM11A could be a result of the higher resolution in the acoustic televiewer in these boreholes, but other reasons to differences is also possible (borehole length, geology and borehole inclination etc.).

**Table 2-3 Distribution of different geometrical classes for the PFL anomalies.**

Borehole ID	Total number of PFL anomalies	Class I	Class II	Class III	Class IV	Class V	Class VI	Class VII
KFM01A	34	11	2	5	12	2	2	0
KFM01D	33	8	0	15	9	0	1	0
KFM02A	102	32	6	21	27	13	0	3
KFM02B	39	8	3	2	19	2	0	5
KFM04A	71	19	5	27	10	0	6	4
KFM05A	24	5	2	9	2	2	2	2
KFM08C	21	14	1	1	3	1	0	1
KFM08D	34	11	4	8	9	1	1	0
KFM10A	52	20	7	15	5	2	2	1
KFM11A	92	41	5	17	24	1	2	2
Sum	502	169	35	120	120	24	16	18
		33.7%	7.0%	23.9%	23.9%	4.8%	3.2%	3.6%

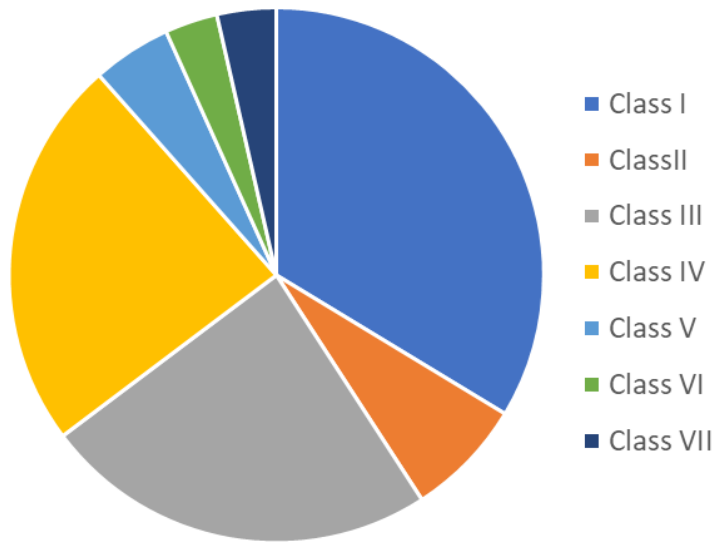


*Figure 2-2. The summed distribution of the geometrical classes I-VII in the 10 classified boreholes (Table 2-3).*

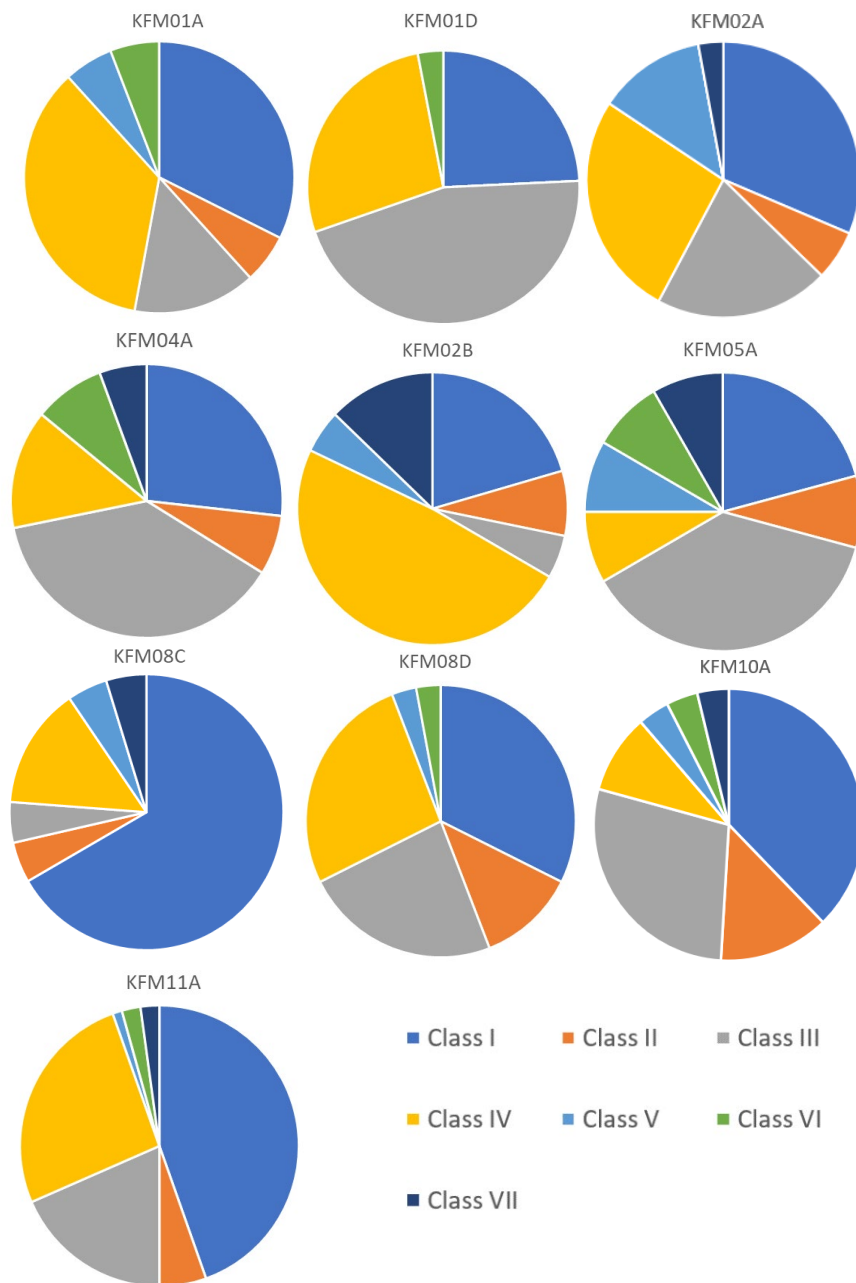


**Figure 2-3.** Distribution of the geometrical classes I-VII in different boreholes (Table 2-3).

## 2.3 Correlations between geometry class and transmissivity

In Table 2-4 the mean of the transmissivity measured in the PFL anomaly section in each geometry class is presented. Figure 2-4 shows the transmissivity for each of the studied PFL-fractures, sorted by the geometrical class given. Note that the y-axis in Figure 2-4 shows the transmissivities in a logarithmic scale. In Figure 2-5 the data is instead shown in the form of number of PFL fractures in each transmissivity interval, for each geometry class. It may be concluded that there is a large spread in transmissivity, of several orders of magnitude, for each class. However, there are also, as expected, many more fractures in geometry class I that are correlated to a low transmissivity ( $< 10^{-8}$ ). The geometry class III and IV have about similar transmissivity span. For the highest geometrical class VII, the number of observations is fairly low, but it seems that some of them do correspond to the highest transmissivities in the boreholes, while some do not. One explanation to the latter cases could be that some of the more complex structural features have gouge or clay infilling that may block the flow but it is prone to be washed out from the borehole wall during drilling, and therefore they may appear more open in the AT image than what they actually are at a certain distance from the borehole wall into the fracture.

Also, it was observed that about half of the most conductive PFL-anomalies ( $> 10^{-7} \text{ m}^2/\text{s}$ ) correspond to simple single fracture planes, i.e. PFL-fractures with geometry classes I-III; and, likewise, to the class IV which has also a fairly simple geometry (2-3 close fractures). Therefore, this shows that not only structural features found at fracture zones or “crush” can be highly conductive, but also single fractures are quite common at PFL anomalies. However, it should be remembered that the number of PFL-anomalies are very few compared to the total number of mapped open fractures, and also, that the PFL distribution with depth is not even. The occurrence of PFL anomalies is clearly higher in the upper part of the bedrock, see e.g. (Follin 2008) and Appendix A. This study includes, however, only boreholes sections below ca 100 m depth since these studies focus on sections where the AT log is performed. Therefore, additional differences or characteristics that may exist in the upper part of the bedrock is not covered by this study.

Further, the single fracture aperture is not the only factor that determines the flow. The connectivity between the different neighbouring fractures is also a determinant factor in the measurements using the flow log. The Posiva flow tests are conducted such that they last for a considerable time, and therefore, the test results are influenced by the fracture aperture conditions also in an area far out from the borehole itself, and not only by the aperture at the borehole intersection. This may explain the spread of transmissivity measured for PFL-fractures that appear geometrically fairly similar from the televiewer image of the borehole wall at the intersection.

**Table 2-4. Mean and median of transmissivities measured at PFL-anomalies for the PFL-fracture geometrical classes.**

Geometry class	I	II	III	IV	V	VI	VII
Number of PFL-fractures.	169	35	120	120	24	16	18
Arithmetic mean of transmissivity ( $\text{m}^2/\text{s}$ )	$0.14 \times 10^{-6}$	$1.09 \times 10^{-6}$	$1.28 \times 10^{-6}$	$0.95 \times 10^{-6}$	$2.90 \times 10^{-6}$	$2.36 \times 10^{-6}$	$7.10 \times 10^{-6}$
Median value of transmissivity ( $\text{m}^2/\text{s}$ )	$0.007 \times 10^{-6}$	$0.028 \times 10^{-6}$	$0.056 \times 10^{-6}$	$0.034 \times 10^{-6}$	$0.095 \times 10^{-6}$	$0.047 \times 10^{-6}$	$3.55 \times 10^{-6}$

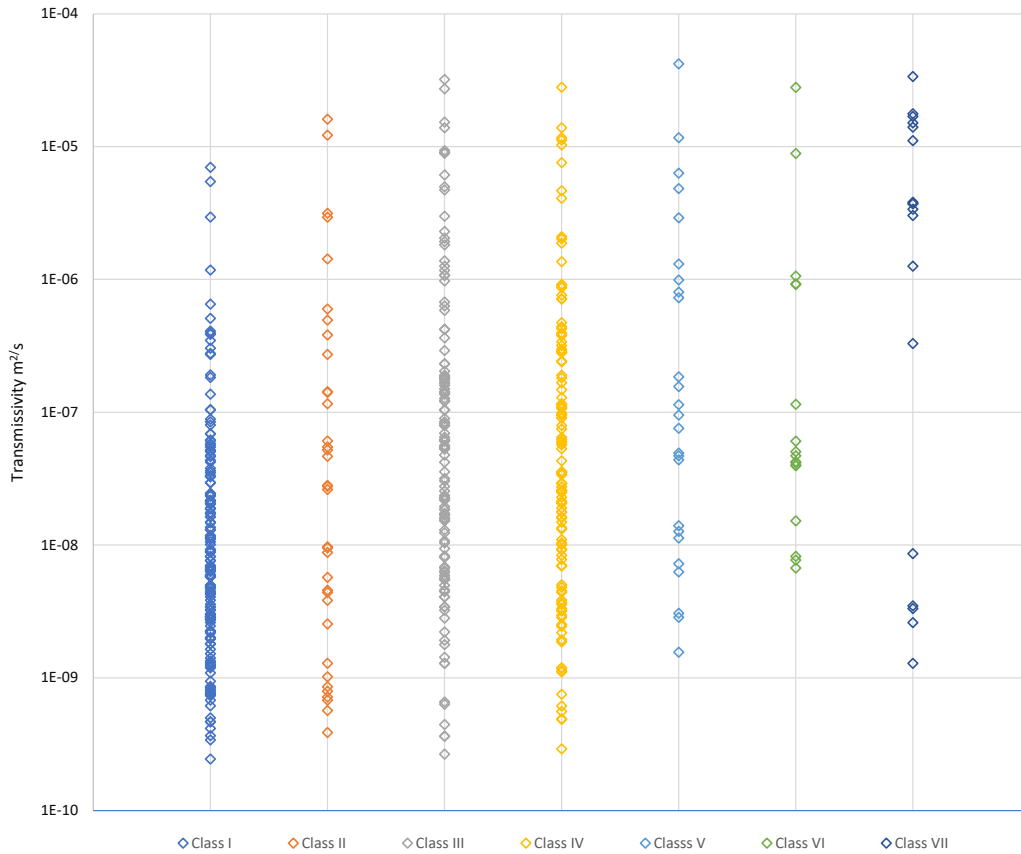


**Figure 2-4.** The measured PFL anomaly transmissivity vs the geometry class of the corresponding PFL-fracture. Geometry class explained in **Table 2-2**.

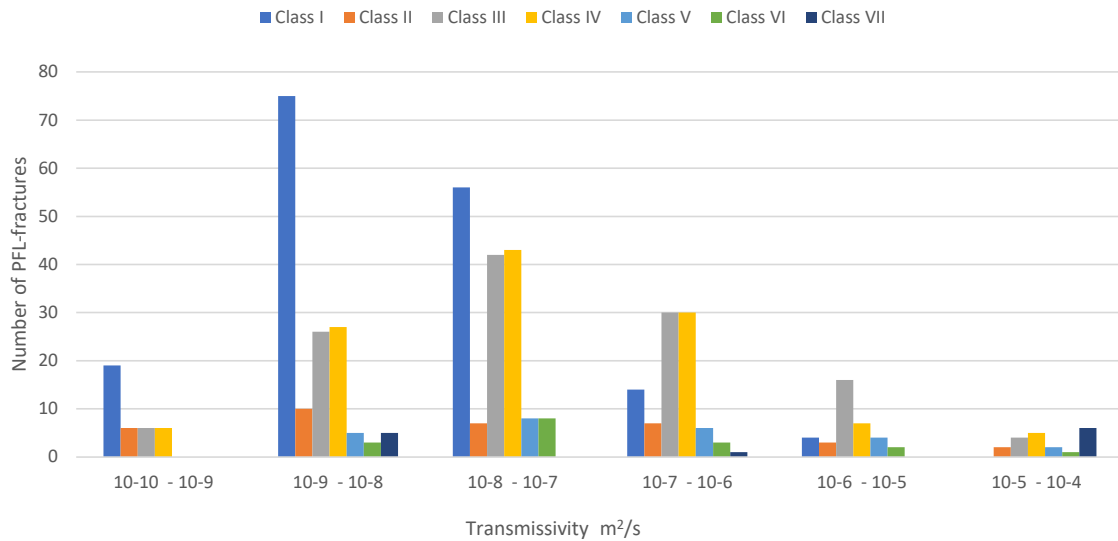


**Figure 2-5.** Distribution of transmissivity for the different geometry classes of PFL-fractures. Notice that the relatively few fractures in the lowest group is close to the measurement limit, and thus the criterion for having a PFL-fracture.

### 3 Comparison of Boremap parameters for PFL-fractures and the other open fractures

#### 3.1 Data set included in study

All Forsmark investigation boreholes where *both* Posiva Flow Log and acoustic televiewer log have been applied were included in the comparison between PFL-fractures and the total population of natural open fractures. These boreholes are KFM01A, KFM01D, KFM02A, KFM02B, KFM04A, KFM05A, KFM08C, KFM08D, KFM10A and KFM11A (Figure 3-1). The open fractures are identified in SICADA as fractures with apertures larger than zero. The natural fractures with aperture equal to zero are denoted sealed and they have not been considered in this study. The very seldom occurring “partly open” fractures are also not included in the study because they do not have surface characteristic parameters mapped. In the comparison, the mapped characteristics of the PFL-fractures are compared with the characteristics of the “Non-PFL open” fractures in the same borehole sections (i.e. not the upper ca 100 m parts of boreholes where logging was not performed). The total number of open fractures in all of the selected borehole sections is 7804 and the PFL-fracture out of them is 411, so the “Non-PFL open” fractures are 7393. The same data set is used in this Chapter 3 studies, but it thus differs from sets in Chapter 4 and 5.



**Figure 3-1.** The location of most of the cored boreholes and percussion drilled boreholes. In this study data from boreholes KFM01A, KFM01D, KFM02A, KFM02B, KFM04A, KFM05A (not shown), KFM08C, KFM08D, KFM10A and KFM11A are used.

### 3.2 Surface and roughness

During core mapping according to the Boremap system—defined in method description SKB MD 143.006—each natural open fracture surface is characterized regarding the parameter called “Surface”. It can be either “rough”, “smooth” or “slickensided”. The distribution for these parameters in the population of Non-PFL fractures and the PFL-fractures is presented in Figure 3-2. It may be noted that the percentages for the different parameters are similar for the two groups.

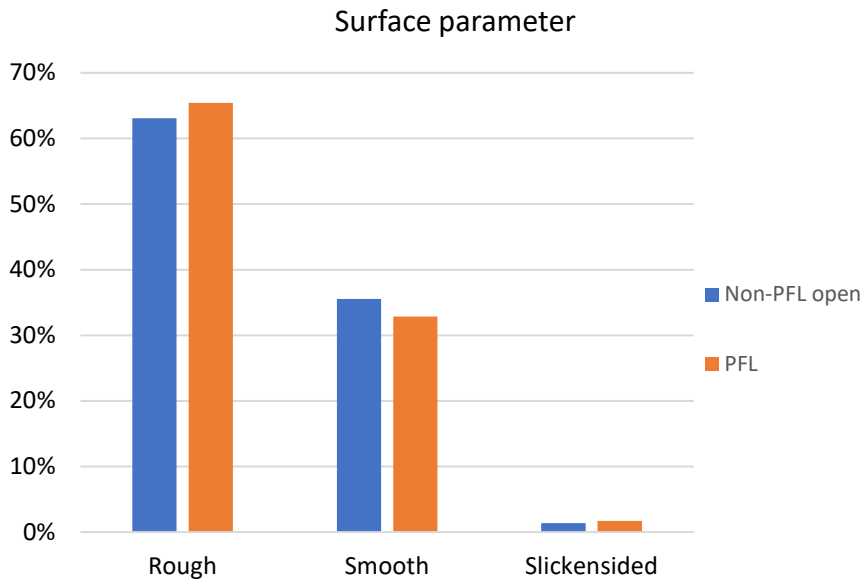


**Figure 3-2.** Distribution of the different “Surface” parameters for Non-PFL open fractures (7393) and for the PFL-fractures (411).

In the same way, the other mapping characteristics, denoted “Roughness” in Boremap, can take the values “planar”, “undulating”, “stepped” and “irregular”. The results of the comparison are shown in Figure 3-3. The distribution of parameters is very similar between the large Non-PFL group and the PFL-fracture group. From this comparison it can be concluded that the single surface itself does not give any enlightenment to differences in flow characteristics. Note here, that these two parameters “Surface” and “Roughness” are determined from the *single* fracture surface with the lowest value or score (worst case) only, and is *not* describing the two opposing surfaces as a pair. And the comparison made suggests that there is no correlation between the single surface characteristics and the matedness (i.e. the aperture distribution) of fractures at the Forsmark site.

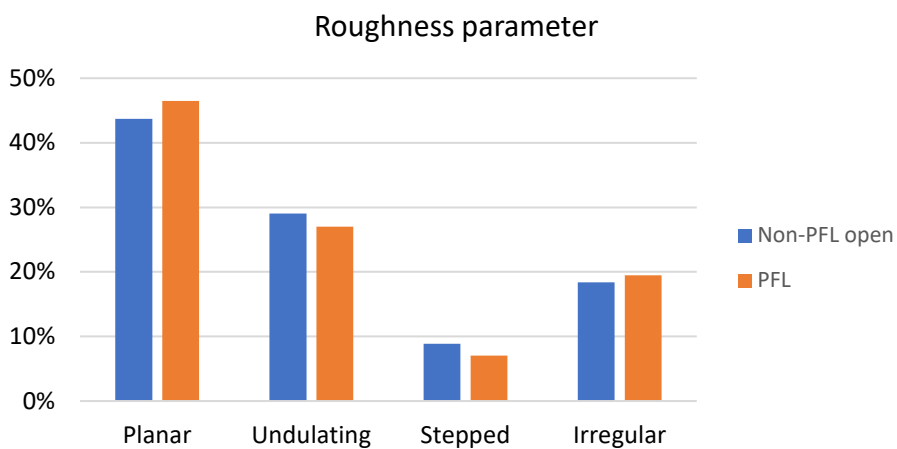


**Figure 3-3.** Distribution of the different “Roughness” parameters for Non-PFL open fractures (7393) and for the PFL-fractures only (411).

### 3.3 Joint alteration and $J_a$

During Boremap mapping the degree of alteration is also mapped in different classes from fresh to as presented in Figure 3-4. A similar parameter for comparison and potential correlation to PFL-fractures is the parameter “Joint alteration”,  $J_a$ . It is an empirical parameter that takes on numerical values according to the degree of alteration (Barton, 2002), so it is almost the same as the other parameter but with a numerical value. The distribution of  $J_a$  is shown in percentage for Non-PFL and PFL-fractures in Figure 3-5. For both groups, about half of them have a  $J_a$  number of 1, which corresponds to the description “unaltered joint walls, surface staining only”. The distribution in general is very similar between the compared groups. This indicates that whether a fracture is belonging to the PFL group or the group of other open fractures today is not significantly coupled to the degree of alteration. A possible explanation to this could be that the alteration is a result of geological processes from the whole geological history long time span, while the aperture is more dependent on the latest tectonics and movements.

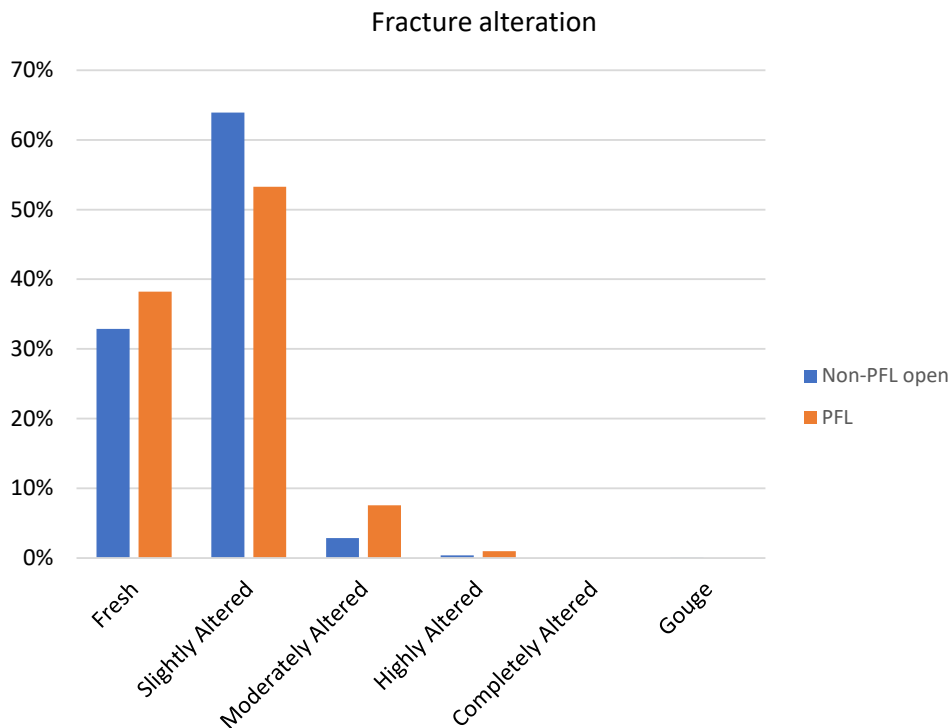


*Figure 3-4. Distribution of alteration class mapped for Non-PFL fractures (7393) and for PFL-fractures (411).*

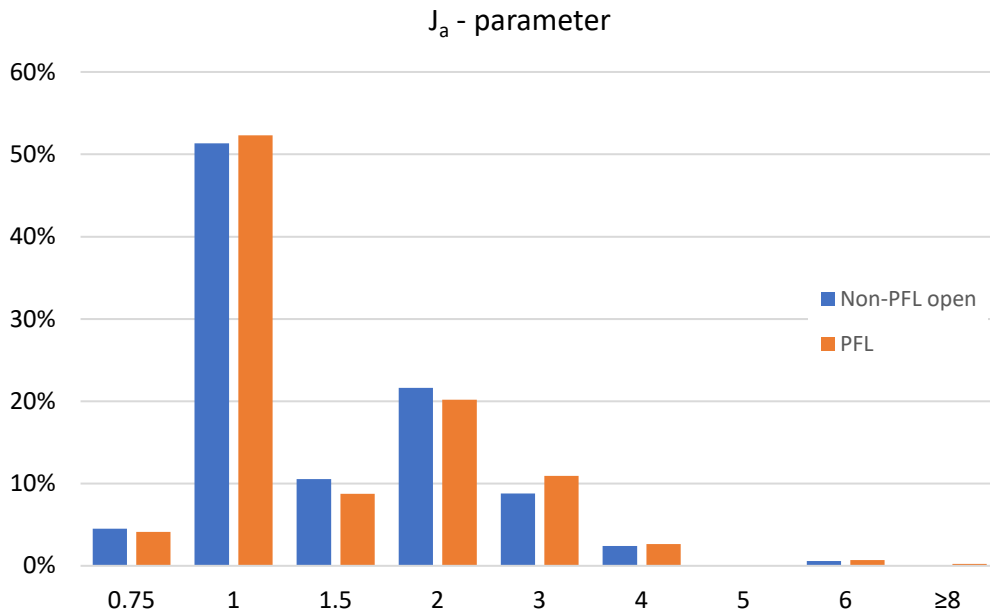


Figure 3-5. Distribution of Ja values for Non-PFL open fractures (7393) and for the PFL-fractures (411).

### 3.4 Fracture aperture

During core mapping, the images from BIPS-logging are used to identify and orient all the natural fractures. In the cases with larger apertures, an estimation of the characteristic aperture is made by a measuring tool in Boremap. The accuracy of this measurement is limited to the pixel size in the image, the variation in image quality and fracture orientation. However, the closest judged value in mm is registered. All open fractures with apertures smaller than measurable, that is 1 mm, are given the same default value 0.5 mm according to the method description for the Boremap mapping system, SKB internal controlling document SKB MD 143.006.

In Figure 3-6 the number of fractures mapped with the different apertures are presented (only borehole sections where PFL-fractures has been identified is included in this comparison). The total number of Non-PFL fracture is of course much larger than the number of PFL-fractures. Therefore the comparison is easier to make in a diagram with the distribution in percentage of the total number in each group. The majority of the the Non-PFL open fractures (88 %) do not have a measurable aperture in the BIPS-images, Figure 3-7. This category is clearly smaller (36 %) for the PFL-fractures.

Note that these BIPS-images used for the Boremap aperture parameter are not the same images as the acoustic logging (AT) images presented previously in Section 2.1. Also, one should remember here that only one (1) of the fractures in the PFL anomaly borehole section is pointed out as “the best choice”, i.e. as being “The PFL fracture”. In some flow logged section there could be several fractures with a fairly high aperture (cf. Chapter 2), but in this comparison in Chapter 3 only the “best choice” (the PFL fracture) are compared to all the other open, including those that are inside a PFL anomaly.

From this comparison it can be concluded that most (64 %), but not all, PFL-fractures have been found in the BIPS-image as fractures with aperture equal to or larger than 1 mm. The percentage of these fractures, with apertures of 1mm or larger, is clearly higher among the PFL-fractures compared to the Non-PFL open fractures. This means that the aperture, as expected, is a main controlling factor for highly water conductive fractures. However, since the total number of Non-PFL fractures is so large it is not possible to simply use the mapped aperture only to *identify* PFL-fractures in a borehole. As can be seen from the comparison in Figure 3-6 the number of Non-PFL fractures with aperture 1mm or more is still more than the total number of PFL fractures.

There could be many explanations to this, for example: 1) The aperture at the borehole is not the only parameter determining the flow into the borehole during the Posiva flow logging. Also fracture connectivity and apertures at a distance from the borehole influences the measured flow, 2) The accuracy of the aperture parameter measurement in the Boremap procedure is low and fairly subjective, 3) It is hard to select a single representative aperture value from fractures with complex structural features in the BIPS-image, 4) The open part of the fracture trace in the image is dark, which may instead of a void be a dark infilling mineral in the fracture, 5) Only one “best choice” fractures are pointed out in the PFL anomaly section as the dominating “PFL-fracture” and any other open fracture is in the Non-PFL group, irrespective of mapped aperture.

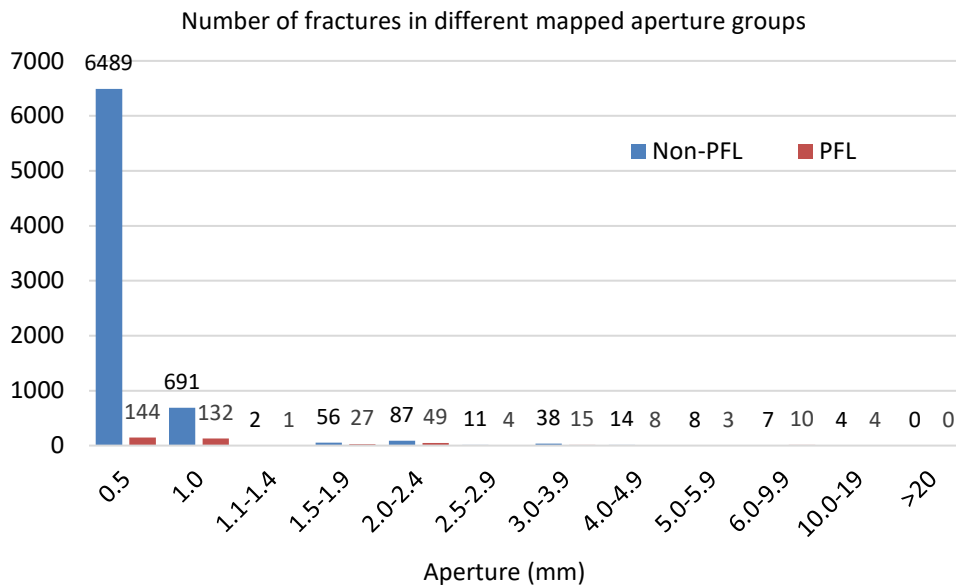


**Figure 3-6.** Distribution of apertures estimated from BIPS images during Boremap mapping. The number of mapped fractures in each group is given above the bars.

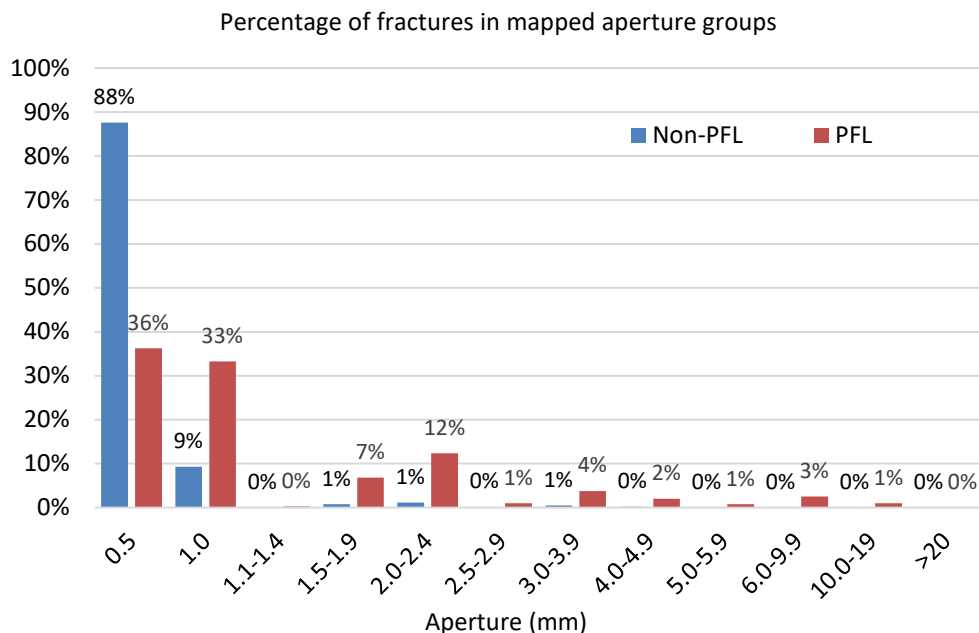


**Figure 3-7.** Percentage of fractures mapped apertures estimated from BIPS images during Boremap mapping.

### 3.5 Fracture mineral

To further compare the PFL-fracture characteristics to other open fractures, the main fracture infilling mineral was obtained from Boremap data SICADA (p\_fract\_core). Most fractures have more than one mineral infilling and, in the Boremap mapping system, the mineral judged to have the largest volume is denoted by “Mineral 1” (MIN1), the next is denoted by “Mineral 2” and so on. In this study only the distribution of Mineral 1 has been compared, the Non-PFL open fractures and for the PFL, respectively, in the studied boreholes (Figure 3-8).

Most fractures have either chlorite or calcite as the main infilling mineral, and this is the case irrespective of being Non-PFL or PFL fractures. Note that this compilation is only about the *type* of *main* infilling mineral, not the amount of the different infilling minerals. The standard Boremap mapping just include a rough estimation of the average total width of the fracture (including aperture and fracture mineral width), but a special study has previously been made for certain borehole sections regarding the amount of the different fracture infillings (See further in Section 5.6).

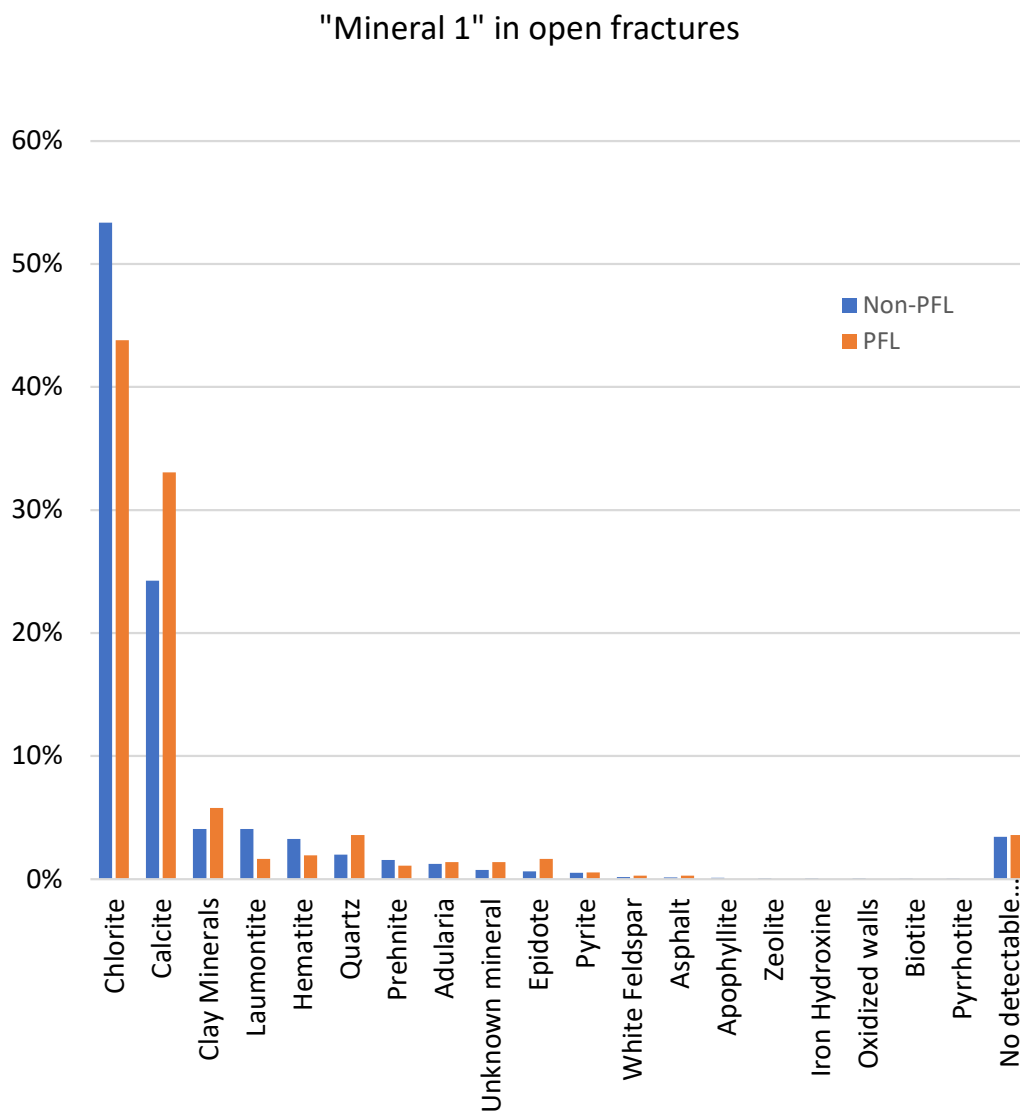


**Figure 3-8.** Distribution of main infilling mineral (MIN1) in the Boremap mapping (note that most fractures have more than one infilling mineral and Min1 is the mineral judged having the largest volume on the surface). The total number of “Non-PFL” open fractures in the borehole sections included in this comparison is 6892 and the number of PFL-fractures is 363.

The distribution between different main minerals looks similar for the Non-PFL and the PFL fractures with some minor differences. Laumontite and hematite is less common as the dominating mineral of the PFL-fractures while clay minerals and quartz are more common as main mineral for PFL-fractures compared to Non-PFL fractures.

Interestingly there are fractures without *any* detectable mineral that are also PFL-fractures. A special study of these fractures without any mineral infilling is previously made by Claesson Liljedahl et al. (2011). After analysing these fractures, they concluded that many of them actually contained minerals, but in very small amounts only possible to detect using scanning electron microscope. For some of these fracture surfaces only a few microscopic crystals were detected. Different possible explanations to this rare type of PFL-fractures are discussed in detail by Claesson Liljedahl et al. (2011).

Extensive and specifically directed studies of the fracture mineralogy at Forsmark were performed by Sandström et al. (2008) and Sandström and Tullborg (2011) as a part of the Forsmark site investigations. Four different generations of fracture mineralisation were distinguished. Generation 4 is dominated by chlorite/clay minerals and thin precipitates of calcite in predominantly hydraulic conductive fractures and fracture zones. They further concluded that many fractures are reactivated and that most of the transmissive fractures have been water conductive during a very long period of time which indicates that a high degree of stability exists in the fracture systems and that newly formed transmissive fractures are rare.

These findings, and the conceptual geological evolution in the site, should be considered when the mechanical properties of the different types of fractures are evaluated.

## 4 Surface matedness of PFL-fractures

### 4.1 Matedness – Aperture spatial correlation

As shown in Section 3-2 and 3-3, no particular differences were found when comparing the mapped surface characteristic of the PFL-fractures and the other open fractures in the same borehole sections. Also, the infilling mineralogy was shown to be similar in the two groups, even if slightly more infilling might be expected on the PFL-fractures, on average (Section 3.5).

In general, the explanation of the difference in transmissivity between - PFL-fractures is a result of difference in aperture and/or in fracture connectivity between flowing fractures in the PFL-anomaly. The study of AT-class (presented in Section 2.1) showed that it was possible to identify the fractures with flow above the PFL measurement limit using the acoustic televiewer log. In all cases a fracture was observed in the AT image at the approximate same borehole depth. However, there are also fractures with larger aperture in the images (BIPS or AT) that are not pointed out as PFL-fractures (see Figure 3-7). This can be explained by several factors or circumstances: 1) The fracture may be located inside the PFL anomaly but not selected as the “best choice” in the section (there may be several open fractures in a single PFL anomaly but only one is selected to be the “best choice”, i.e. the PFL-fracture), 2) The fracture may have been filled with soft mineral (clay) that has been washed out such that it appears open in the borehole wall images but the actual undisturbed aperture is smaller further into the rock, or even that the fracture is there totally clogged, 3) The fracture may have a poor connectivity to other flowing fractures, resulting in a low flow in the measurement, 4) There are sources of uncertainty in the correlation of “best choice” due to length correlation difficulties.

Nevertheless, that there is a large variety in mean aperture and aperture distribution between different fractures in the rock mass is without doubt. The question then remains how to explain this difference in apertures between different fractures. In general, it can be said that it is explained by the difference in geological history, which determines the generation, propagation and relative displacements of the fracture surfaces. Shear movements of fractures will make the opposing points of the surfaces less matching, here denoted having less “matedness”. The longer the shear movement, and the more shearing events, the less mated the fractures surfaces would become. To investigate the matedness explanation for transmissivity differences at Forsmark, it was of interest to try to find some way to observe matedness difference in the drill core fracture samples.

As a very simple fast method to try to observe matedness, between the upper and lower side surface of the fracture, an attempt was made using a profilometer (the type of metal “comb” usually used to estimate the joint roughness coefficient, JRC, Barton and Choubey 1977). This profile is not very accurate since it stems from a limited number of “comb pins” and the line is drawn by hand with a pen. Furthermore, the location of the opposing profiles is not easy to select accurately. Still, the surface character is shown quite well with this method, and at least the clearly mated surfaces can be distinguished from the clearly unmated pairs.

The trial of this matedness study with profilometer was carried out on the PFL-fractures in KFM10A, with the exception of the fractures where measurements were not possible due to a significantly damaged surface on either side. The result is presented in Table 4-1. Note that the placement of the two profile lines (angle and distance) in the image column of the table has no relevance. They are just drawn separately at approximately correct side-wise position such that the profile geometries can be compared. The PFL-fractures in the table are presented in the order of increasing transmissivity of the corresponding PFL-anomaly, which means that the first fracture sample in the table had the lowest flow into the borehole.

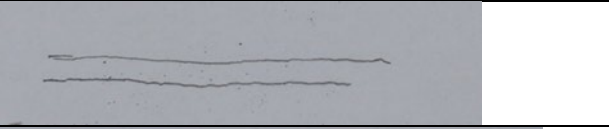
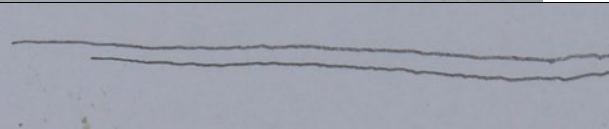
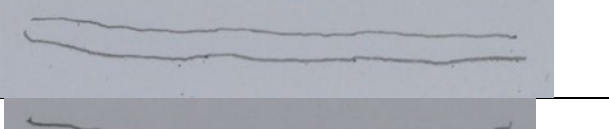
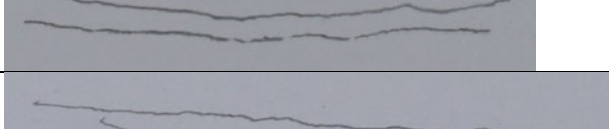
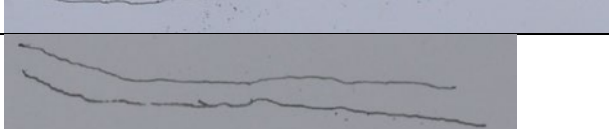
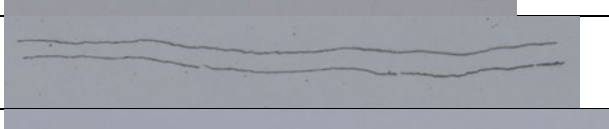
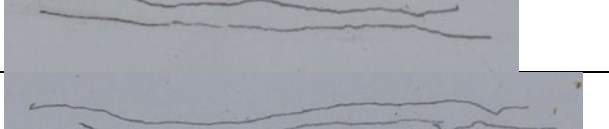
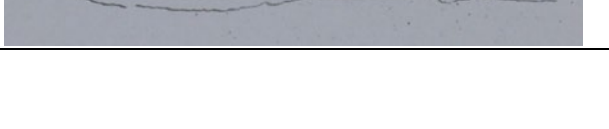
The table also gives the AT-class that was estimated from the acoustic televiewer log. Note that this is interesting in the way that the matedness judgement, based on profilometer readings, requires only the core in the box, and the AT-class is based solely on the acoustic televiewer image from the cored borehole. Further the aperture estimated during the Boremap logging is given in the table, and this estimate is made from the BIPS-image (as aforementioned, the accuracy of these BIPS based estimates is low, because of the size of single pixels, with the aperture value of 0.5 mm set as a default for all fractures where the aperture is judged small (less than 1 mm) but still open to flow). Therefore, these different methods/estimates are fully independent from each other and from the Posiva Flow Log measurements, which gives the transmissivity value for the corresponding section of the borehole.

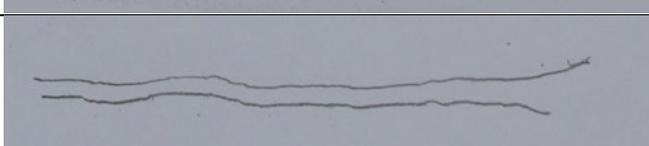
Although too few fractures are measured to give a certain support to the observations, it seems that there is a correlation between the different measurements, as expected. The PFL-fractures with transmissivity of the order  $10^{-8}$  m<sup>2</sup>/s are mostly AT-class I and have mated surface profiles. The fractures with transmissivity  $10^{-7}$  m<sup>2</sup>/s have mostly AT-class II or III and their profiles seem less clearly mated. Out of the two most water conductive fractures (with transmissivity over  $10^{-6}$ ), the anomaly with ID 50 has clearly unmated surface profiles and AT-class III. The other most conductive PFL-fracture (ID 15) has unclear matedness and AT-class IV, i.e. the PFL-anomaly is judged from the AT-log to consist of several closely located water bearing fractures.

According to Section 2.2, there is generally a part of PFL anomalies (ca 30 %) that are not located at a single fracture plane (geometry Classes IV-VII) and their matedness cannot be measured, or defined, for such structural features.

The results from this trial study with profilometer indicates that there could be a benefit in measuring opposing fracture surface geometry and determine the matedness more accurately, such as with a 3D laser scanner, to improve the understanding of hydro-mechanical properties of fractures. In particular this may be of interest when detailed flow loggings are not available. In such future studies the matedness of PFL-fractures could also be compared to matedness in the group of Non-PFL fractures.

**Table 4-1. Results from the measurement with profilometer on PFL-fractures in KFM010A.**  
 See text for explanation.

PFL Anom. No	Transmissivity (m <sup>2</sup> /s)	Opposite profiles in centre of fracture core sample. Profile length is 5cm – 10 cm.	AT Geom. Class	Aperture from BIPS (mm)
25	5.79×10 <sup>-9</sup>		I	0.5
26	1.18×10 <sup>-8</sup>		I	1
52	1.63×10 <sup>-8</sup>		I	0.5
41	1.95×10 <sup>-8</sup>		III	0.5*
53	2.04×10 <sup>-8</sup>		I	0.5
29	2.06×10 <sup>-8</sup>		I	0.5
3	2.17×10 <sup>-8</sup>		I	0.5
42	2.25×10 <sup>-8</sup>		III	1
54	2.36×10 <sup>-8</sup>		I	0.5
20	5.48×10 <sup>-8</sup>		II	0.5
44	5.63×10 <sup>-8</sup>		III	2.5
31	6.10×10 <sup>-8</sup>		I	1
7	1.16×10 <sup>-7</sup>		II	1.7
18	1.37×10 <sup>-7</sup>		I	0.5
38	2.04×10 <sup>-7</sup>		III	1.5

PFL Anom. No	Transmissivity (m <sup>2</sup> /s)	Opposite profiles in centre of fracture core sample. Profile length is 5cm – 10 cm.	AT Geom. Class	Aperture from BIPS (mm)
17	3.64×10 <sup>-7</sup>		III	1
14	3.82×10 <sup>-7</sup>		II	0.5*
50	1.26×10 <sup>-6</sup>		III	1
15	2.94×10 <sup>-6</sup>		IV	0.5**

\* From BIPS image, it appears more open. Boremap value possibly erratic.

\*\* The explanation to this low Boremap aperture value is probably that the PFL anomaly is located at several fractures and that one of these have appeared to have small aperture in the BIPS image, while the flow corresponds to all of these fractures together.

## 4.2 Aperture measurement using viscous silicon

Another small trial to characterize aperture or aperture matedness was made within the study. This approach consists in applying the technique by Hakami (1992) that used small volumes of viscous silicon being compressed between the fracture surfaces. The measured volume divided by the measured area of the spot covered by the silicon, as it is squeezed out between the surfaces, is a simple way of estimating the average aperture of the spot.

However, in our case it was found that the type of silicon material available had a too low density, was too sticky and with tendency to keep bubbles. It was therefore difficult to accurately make the required tiny ball with a known volume. If the used volume becomes too large it will be difficult to compress the surfaces to a repeatable position with the two surfaces in contact. The attempt to use this measurement method was therefore abandoned.

Also, this approach to measure aperture and aperture variations assumes that the surfaces are under compression at the location, which is not the case for the PFL fractures at the borehole. The acoustic televiewer studies (Section 2.1) indicates that many, if not all, of the PFL-fractures are not in contact at the point of the borehole. The method of silicon compressed volumes may therefore not be able to give much useful information, even if it could possibly have distinguished the very mated fractures from the clearly non-mated fractures (when surfaces are not totally smooth and planar).

## 5 Surface hardness studies using Leeb Hardness Test (LHT)

### 5.1 Instrument and methodology

The Leeb hardness test (LHT) is a rebound test originally developed for metals, that has been increasingly used in rock engineering. The method is based on the dynamic impact principle, where the ratio of the rebound velocity to the impact velocity of a spring-loaded impact body on a material surface is recorded, Equation 5-1. The impact body rebounds faster from harder surfaces than softer ones. The resulting test value is denoted  $L_D$ .

$$L_D = \frac{V_{rebound}}{V_{impact}} \times 1000 \quad 5-1$$

The Leeb instrument is small and hand held, and the test procedure fast and non-destructive, which makes it a versatile and convenient device for laboratory tests as well as for field tests. The device used in this study (Figure 5-1) corresponds to the same model of TIME Leeb hardness tester used in Corkum et al (2018) and Jeans (2021).



*Figure 5-1. The instrument for Leeb hardness test.*

The Leeb hardness test can be used on drill cores, block samples, rock outcrops and fractures surfaces. However, no standard exists for the test procedure on rock materials. A correlation of  $L_D$  with the uniaxial compressive strength (UCS) of rock and a compilation of earlier studies are presented in Corkum et al. (2018). An evaluation of the LHT for determining the joint wall compressive strength (JCS) has been presented in Jeans (2021). Corkum et al (2018) also evaluated the required number of impacts per test, size of the test area and size of the test sample, to give a good estimate of  $L_D$ . They concluded that the number of impacts should be between 10 and 20. Over 20 impacts gives a marginal improvement until reaching the number of 50 impacts or greater which provides negligible gains. In order to avoid changes in the surface density due to repeated impacts at the same spot, the recommended number of impacts should be evenly spread within an area of 25-50 mm in diameter. For tests on drill cores with a diameter of 54 mm, the length of the core tested should be at least 22 mm.

## 5.2 LHT on intact rock surfaces from Forsmark

LHT was performed on drill core samples of amphibolite (rock code 102017) and felsic to intermediate metavolcanic rock (rock code 103076) from two different boreholes, KFM08D and KFM11A (Table 5-1, Figure 5-2 and Figure 5-3). The borehole depths correspond to the planned SFK repository depth for KFM08D, and the SFR repository depth for KFM11A.

Samples of each rock type were tested on the cylindrical surface, with the Leeb instrument perpendicular to the core axis, and on cut cross-sections with the device oriented parallel to the core axis. In addition, fresh rock surfaces caused by breaking the drill core, were tested for amphibolite. After the first test round, the samples were saturated with water for seven days, and then new tests were conducted on the same cut cross-sections. The upper limit of the measuring range was set to  $L_D = 976$ , which corresponds to the scale with the highest possible value in the Leeb hammer device used in the present study. The lower limit for this scale is  $L_D = 80$ . The testing with LHT was continued until at least 12 values were achieved inside the range (with some exception), followed by the calculation of their mean value. The numbers of impacts above and below the measurement limits, respectively, were also recorded.

**Table 5-1. Sample interval for amphibolite in KFM08D and metavolcanic rock in KFM11A.**

Amphibolite (102017)			Metavolcanic rock (103076)		
Borehole ID	Sample nr	Borehole interval (m)	Borehole ID	Sample nr	Borehole interval (m)
KFM08D	1	316.74–316.89	KFM11A	1	173.18–173.33
KFM08D	2	394.70–394.85	KFM11A	2	193.17–193.29
KFM08D	3	480.50–480.65	KFM11A	3	204.30–204.47
KFM08D	4	572.20–572.36	KFM11A	4	211.60–211.74
KFM08D	5	583.50–583.65	KFM11A	5	226.07–226.22

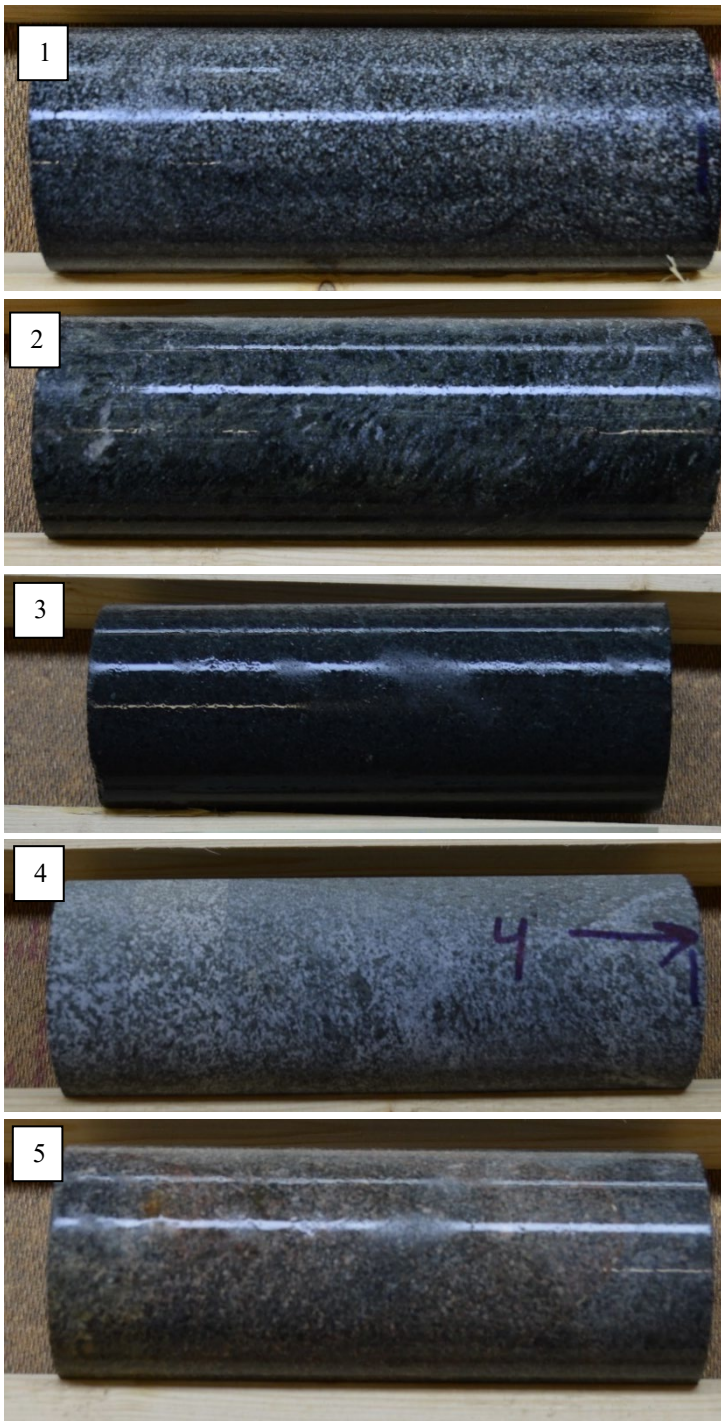


*Figure 5-2. Amphibolite samples for Leeb hardness tests, number 1-5, from KFM08D.*

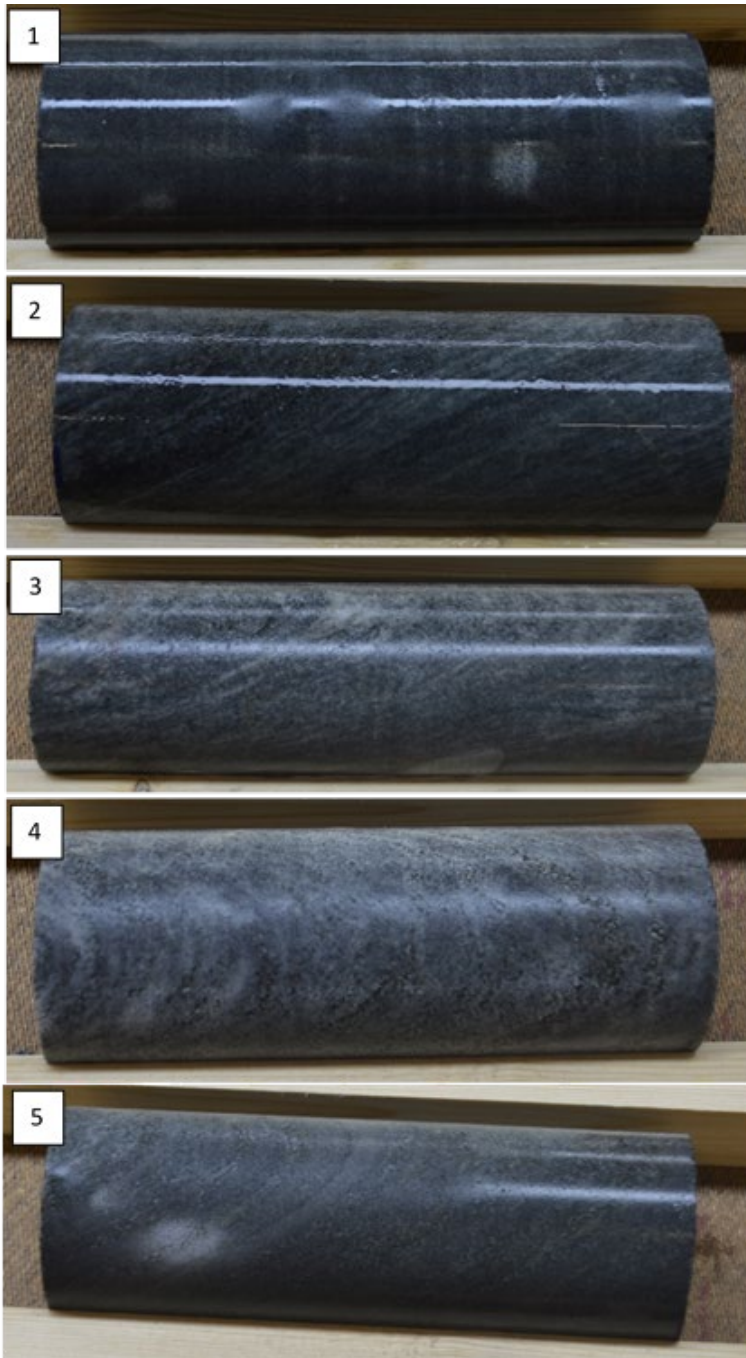


*Figure 5-3. Metavolcanic rock samples for Leeb hardness test, number 1-5, from KFM11A.*

The result for the amphibolite rock type is shown in Table 5-2 and Figure 5-4. The results for the three different tests, cylindrical, cut cross-section and water saturated cut cross-section tests, are quite concentrated for each sample. An exception is the result of the cylindrical test on sample 1. A likely explanation is that this was the first test in which the Leeb hammer device was used, and some handling practice is required to get an optimal impact on the curved surface. The cut cross-sections give the highest results for four out of five samples, which is reasonable since the rounding of the drill core in the cylindrical test, as stated above, makes it difficult to achieve an optimal impact with the Leeb instrument. No significant difference is seen between dry and water-saturated samples.

The highest measurement limit of the specific Leeb device used in this study is somewhat too low for the amphibolite, which results in a number of impacts above the measurement limit, denoted as AML in Table 5-2. Corkum et al (2018) recommended a 12-impact trimmed mean approach, where the highest and lowest values are removed to reduce the impact of possible outlier data given the variability of surface conditions. However due to these observed AML-impacts, no trimmed mean value was used, instead the mean value was calculated on all successful impacts within the measurement limit. The calculated averages for tests with several AML-impacts are therefore not fully representative. The highest test result is obtained for sample number 5, which is also the sample with the most AML-impacts. This is explained by the fact that the sample does not consist of solely amphibolite, but also of granite which is a harder rock type.

The artificially broken rough cross-sections turned out to be too rough (Figure 5-5) for the Leeb instrument to function properly. The values became very low compared to the cylindrical and cut cross-section tests, and a large number of values ended up below the lower measurement limit, denoted as BML in Table 5-2. For sample number 3, there was no available rough surface adjacent to the sample.

**Table 5-2. LHT-results from cylindrical, cut cross-section, water saturated cut cross-section and rough cross-section tests on amphibolite (102017) in KFM08D.**

<b>Amphibolite</b>	<b>Total number of impacts</b>	<b>Average value (L<sub>D</sub>)</b>	<b>Standard deviation</b>	<b>L<sub>D</sub> Max/ L<sub>D</sub> Min</b>	<b>Percentage of AML</b>	<b>Percentage of BML</b>
<b><i>Cylindrical test</i></b>						
Sample 1	14	469	186	738/117	0	0
Sample 2	14	714	96	833/560	14	0
Sample 3	12	702	75	832/590	0	0
Sample 4	14	630	124	791/382	14	0
Sample 5	20	844	109	954/617	40	0
<b><i>Cut cross-section test</i></b>						
Sample 1	13	746	76	871/618	0	0
Sample 2	15	787	102	952/670	20	0
Sample 3	13	708	83	813/555	8	0
Sample 4	14	595	138	870/399	0	0
Sample 5	23	897	51	953/815	48	0
<b><i>Water-saturated cross-section test</i></b>						
Sample 1	13	682	156	951/396	0	0
Sample 2	17	771	120	931/591	30	0
Sample 3	12	739	87	852/626	0	0
Sample 4	13	605	121	807/408	0	0
Sample 5	23	882	61	943/742	48	0
<b><i>Rough cross-section test</i></b>						
Sample 1	17	204	107	377/96	0	29
Sample 2	23	178	82	387/95	0	48
Sample 3	-	-	-	-	-	-
Sample 4	28	137	54	264/83	0	57
Sample 5	25	129	61	273/83	0	52

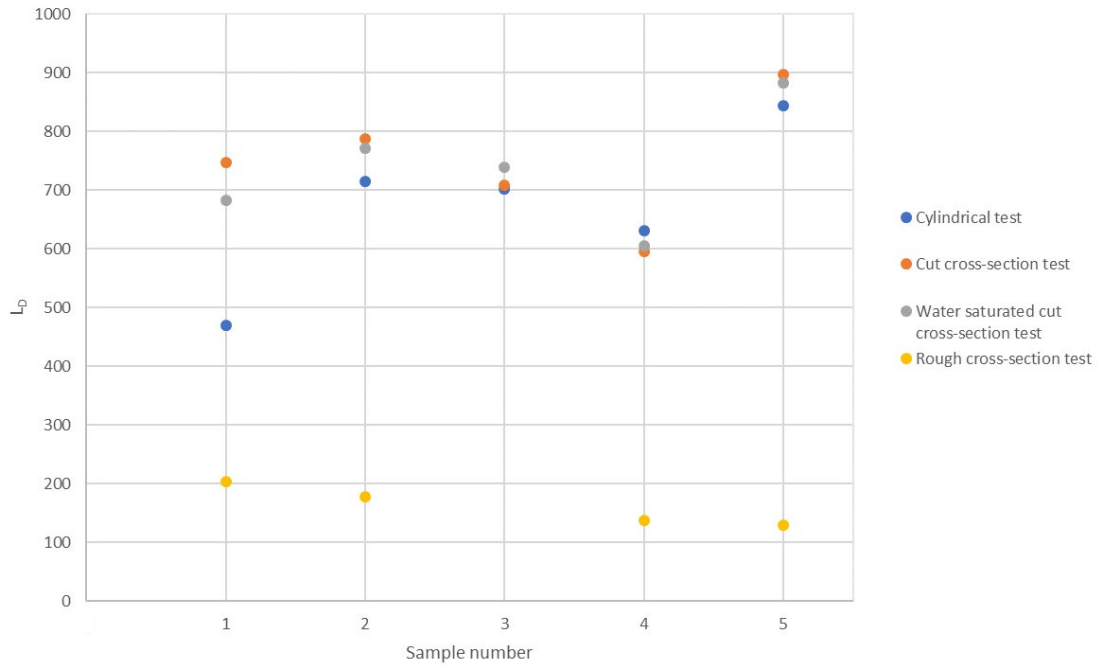


**Figure 5-4.** The LHT average value for amphibolite on different test surfaces.



**Figure 5-5.** Fresh rough cross-section of an artificially broken amphibolite rock core (front and perspective views shown in the left and right figures, respectively).

The result for the metavolcanic rock type is shown in Table 5-3 and Figure 5-6. The metavolcanic rock is harder than the amphibolite, and therefore a large number of impact readings ended up above the upper measurement limit of the Leeb hammer, in particular for tests conducted on the cut cross-sections. The resulting mean values are therefore an underestimate of the hardness of the metavolcanic rock. The cylindrical tests result in lower values for all samples except number 2. Like in the case of amphibolite, the most likely explanation is that the rounding surface of the drill core makes it difficult to achieve an optimal impact. For sample number 1, there are only three successful impact values for the cut cross-section test, all other values are above the measurement limit, and therefore not reported in Figure 5-6. For sample 4 there are also more values above the measurement limit, than values within the measuring range. The spread of the results between the cylindrical and cut cross-section tests for samples number 3-5, is consistent with the visible anisotropic structure in these samples and alteration of biotite, Figure 5-3. Figure 5-7 shows an example of the measurement indentation marks left by the LHT impacts in metavolcanics samples after conducting the cylindrical and cut cross-section tests.

**Table 5-3. LHT-results from cylindrical-, cut cross-section- and water saturated cut cross-section tests on metavolcanics rock (103076) in KFM11A.**

Metavolcanic rock	Total number of impacts	Average value (L <sub>D</sub> )	Standard deviation	L <sub>D</sub> Max/ L <sub>D</sub> Min	Percentage of AML	Percentage of BML
<b>Cylindrical test</b>						
Sample 1	17	909	24	949/869	29	0
Sample 2	19	766	153	955/397	37	0
Sample 3	12	685	179	908/401	0	0
Sample 4	13	730	166	931/666	8	0
Sample 5	12	724	251	951/228	0	0
<b>Cut cross-section</b>						
Sample 1	20	876	51	921//820	85	0
Sample 2	17	766	167	912/451	29	0
Sample 3	19	887	145	941/518	36	0
Sample 4	27	880	78	945/688	56	0
Sample 5	14	825	127	948/535	14	0
<b>Water-saturated cross-section</b>						
Sample 1	26	903	38	945/849	54	0
Sample 2	19	738	218	936/208	37	0
Sample 3	19	797	145	941/518	37	0
Sample 4	26	817	153	930/444	54	0
Sample 5	12	802	156	936/416	0	0

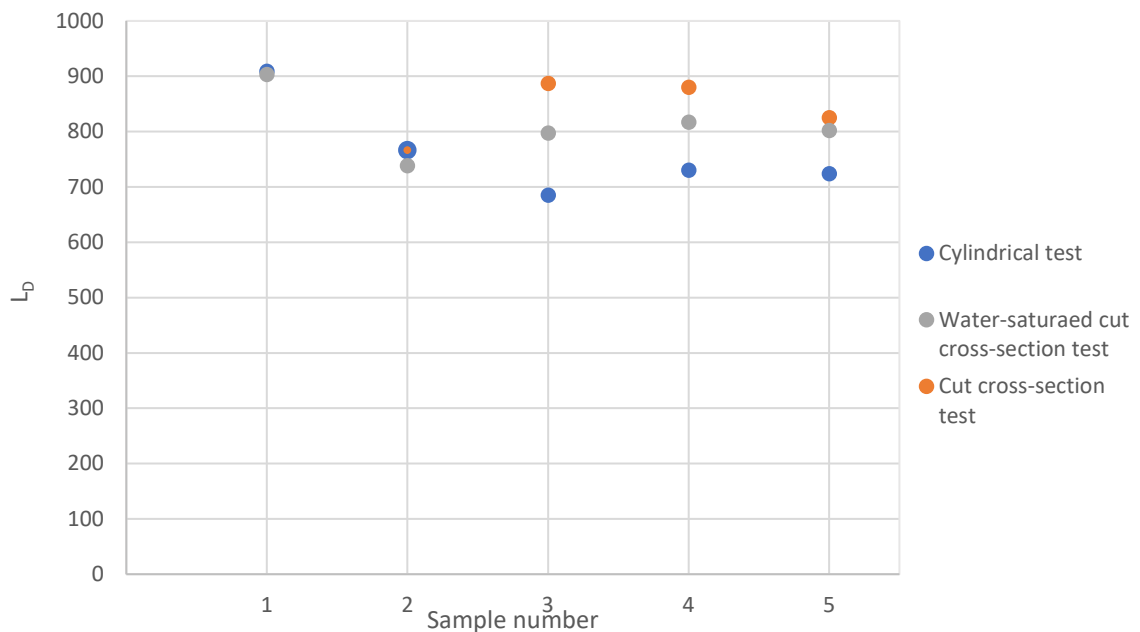


**Figure 5-6. The LHT average value for metavolcanic rock (103076) on different test surfaces.**

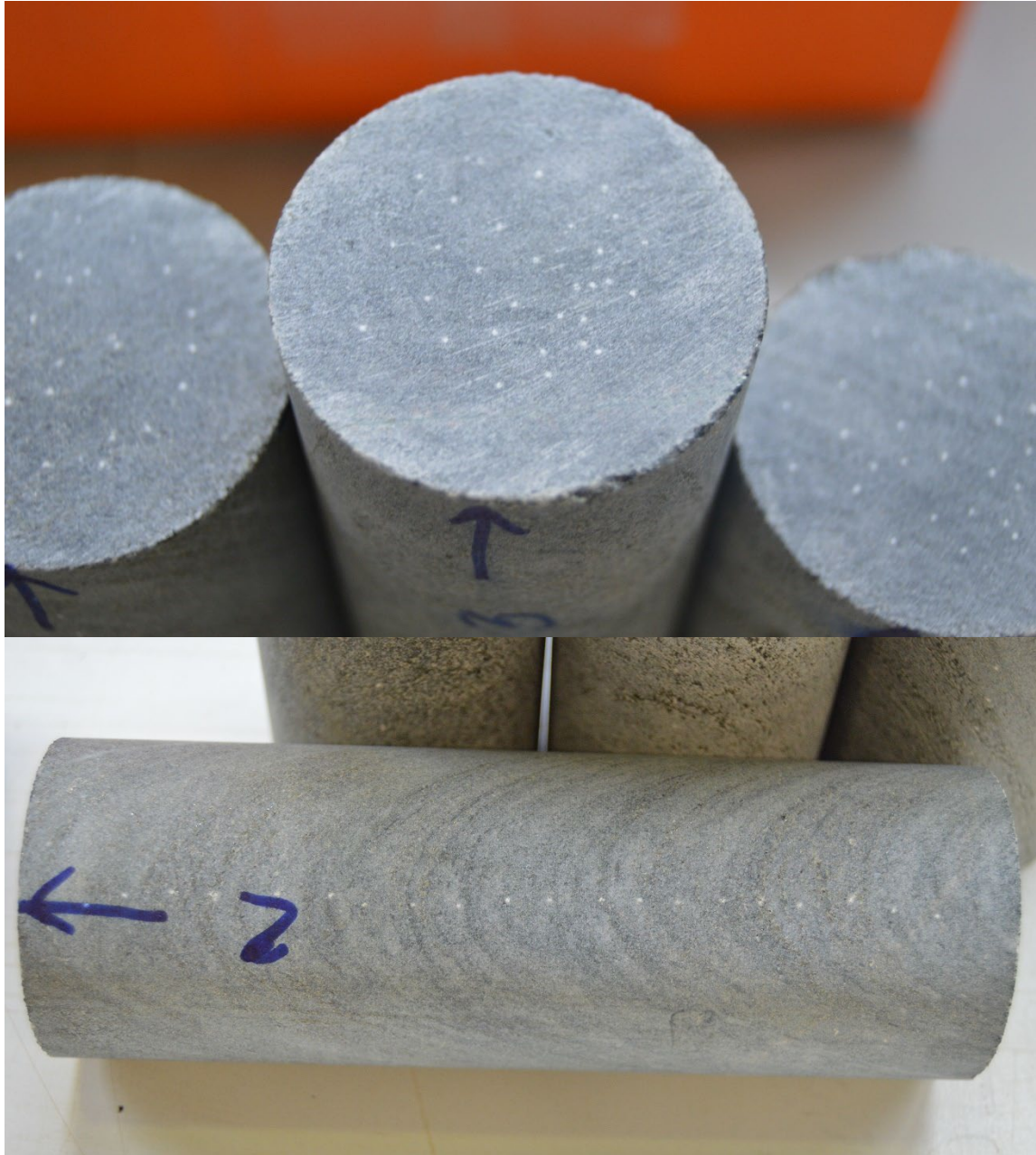


*Figure 5-7. Indentation marks left by LHT impacts in metavolcanics samples after conducting the cut cross-section and cylindrical tests (top and bottom figures, respectively).*

### **5.2.1 Complementary Leeb hardness tests and comparison with UCS and ITS for amphibolite**

A parallel study involving uniaxial compressive strength (UCS) and indirect tensile strength (ITS) testing (Hanquist et al 2023) was conducted during the sampling process of the amphibolite and metavolcanic rocks. In that process, it was decided to complement the LHT measurements for the amphibolite rock case with tests conducted on 5 additional samples, three from KFM08A and two from KFM01A, Table 5-4 and Figure 5-8. Additional tests on metavolcanic rock were not considered, since earlier samples were too hard to get a truly representative hardness value with the LHT due to the upper measurement limit of this particular Leeb device.

The Leeb hardness test (LHT) results for the amphibolite, samples number 6–10, is shown in Table 5-5 and Figure 5-9.

**Table 5-4. Sample interval for UCS, ITS and LHT of amphibolite in KFM01A and KFM08A.**

<b>Amphibolite</b>		
<b>Borehole</b>	<b>Sample nr</b>	<b>Borehole interval (m)</b>
KFM01A	6	260.33–260.55
KFM01A	7	473.45–473.63
KFM08A	8	556.43–556.63
KFM08A	9	900.99–901.18
KFM08A	10	820.93–821.12

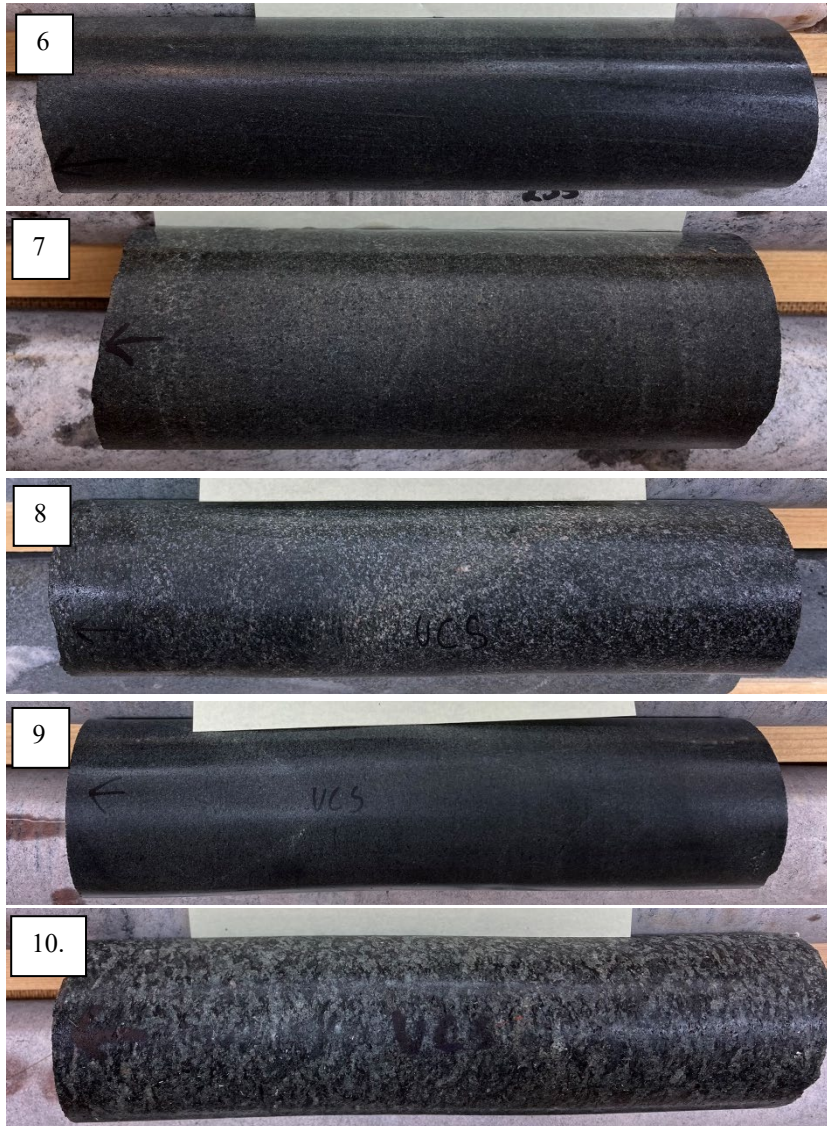


*Figure 5-8. Amphibolite samples, number 6-7 from KFM01A, and number 8-10 from KFM08A.*

**Table 5-5. LHT results for samples in laboratory tests.**

Amphibolite	Total number of impacts	Average value ( $L_D$ )	Standard deviation	$L_D$ Max/ $L_D$ Min	Percentage of AML	Percentage of BML
<b>Cylindrical test</b>						
Sample 6	22	709	78	879/548	5	0
Sample 7	20	756	78	875/604	0	0
Sample 8	22	620	113	828/409	0	0
Sample 9	21	597	126	846/306	0	0
Sample 10	29	219	119	438/87	0	28
<b>Cut cross-section test</b>						
Sample 6	21	770	54	861/618	0	0
Sample 7	25	796	71	949/634	16	0
Sample 8	22	781	78	885/561	0	0
Sample 9	24	715	89	838/445	8	0
Sample 10	23	238	130	474/85	0	13

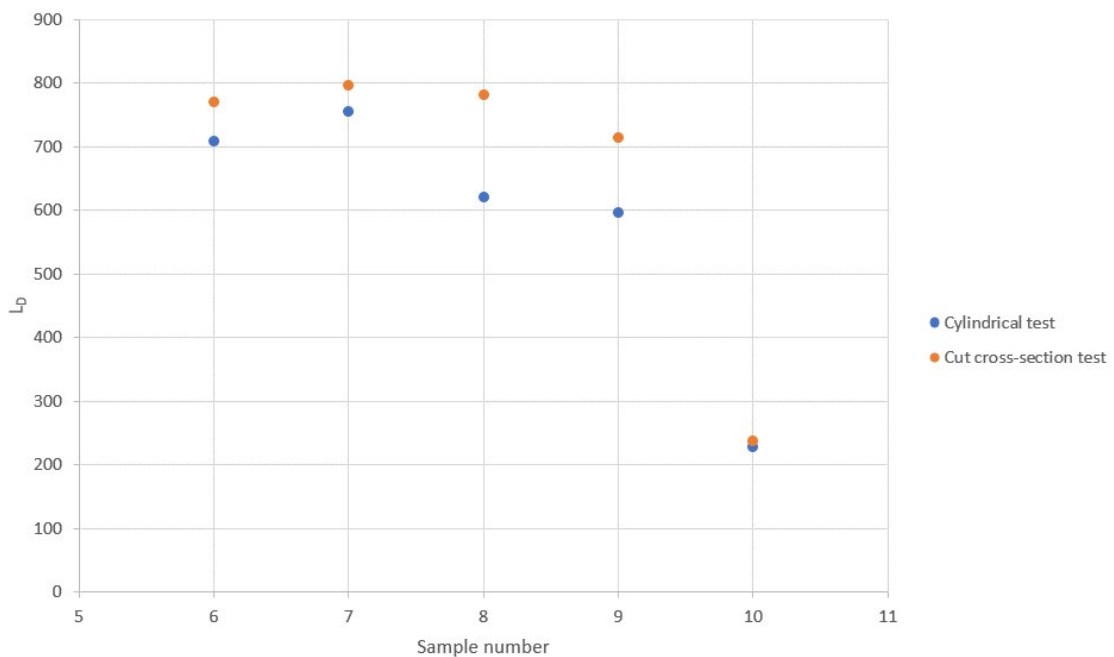


**Figure 5-9.** Results from LHT test on the drill core cylindrical surface and test on cross-sectional cut surfaces of the drill core samples.

Most noticeable in the LHT results for samples number 6–10 are the low values obtained for sample number 10. The impact results are low, showing a large spread, with quite many of them being below the measurement limit. This can be explained by the fact that the sample number 10 is intensely altered by chloritization and have larger grain size than normal, which means that some impacts probably lied on individual weaker mineral grains.

The methods and results from UCS and ITS laboratory tests are reported in detail in Hanquist et al (2023). When the LHT results are compared to the laboratory results from the UCS tests (Figure 5-10) a relationship can be noted between the low  $L_D$  value for sample 10 and its corresponding elastic modulus and strength values. There is also a relationship between the LHT results and the indirect tensile strength values, ITS, obtained from samples located adjacent to the UCS test samples (Figure 5-11). The lowest UCS and ITS values of approximately 44 MPa and 6 MPa, respectively, correspond both to the low mean  $L_D$  of 238.

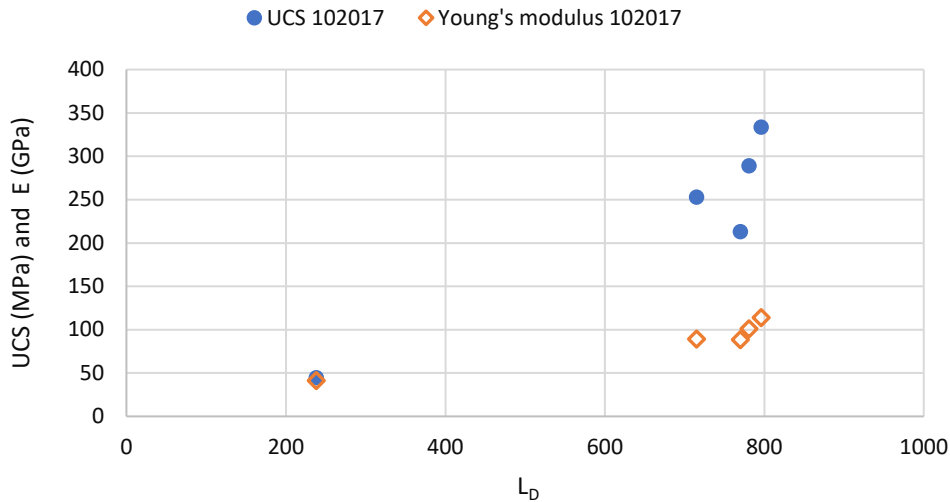


**Figure 5-10.** Cross plot of LHT results and the UCS and Young's modulus results from the laboratory test (Hanquist et al 2023) on five amphibolite (102017) samples in **Table 5-4**.

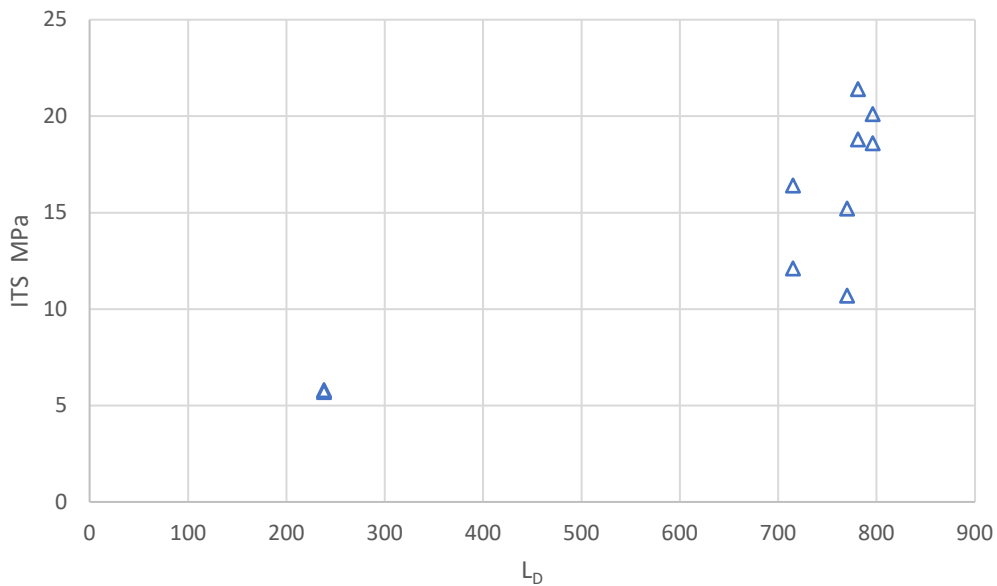


**Figure 5-11.** Cross plot of LHT results and the indirect tensile strength (ITS) test result from ten tests conducted on amphibolite (102017) samples taken at each side of five UCS test samples at different borehole locations (**Table 5-4**).

The LHT tests on the metavolcanic rock resulted in many impacts that were AML (Table 5-3). This implies that the UCS of metavolcanic rock should be higher than the UCS of amphibolite. However, the laboratory results showed that the average UCS for five samples from metavolcanic rock was actually lower (177 MPa) than the average of five amphibolite samples (226 MPa) (Hanquist et al. 2023). On the other hand, the indirect tensile strength was, on the average, higher for the metavolcanic rock (19 MPa) as compared to the amphibolite (14 MPa). This indicates that a further investigation is needed to evaluate the use of LHT to correlate hardness to strength parameters for different rock types.

### 5.3 LHT on PFL-fracture surfaces

Three boreholes, KFM01D, KFM10A and KFM11A, were selected for a more detailed study on PFL-fractures in class I, II and III (see Chapter 2.1.1), and for conducting LHT on their fracture surfaces. The other classes were excluded because they include several fractures or structures, which makes difficult, in practical terms, to test them with LHT. The selection was made based on borehole sections with a detailed mineral mapping (Eklund and Mattsson 2009) and the image quality of the AT-logs. Fractures classified as I-III with a transmissivity of at least  $10^{-8}$  m<sup>2</sup>/s, according to the PFL anomaly, were sorted out for the study. Some of these fractures could not be tested due to missing core pieces, being only partly broken fractures or a highly fractured drill core. A total of 42 PFL-fractures with the correct criteria were tested.

Figure 5-12 shows the transmissivity for these 42 PFL-fractures, divided into geometry class I-III. Class III has fractures with higher mean transmissivity compared to class I and II, consistent with the larger aperture observed in the AT images for this class.

The results of the LHT are presented in Table 5-6 and Figure 5-13 and Figure 5-14. Photographs of the tested fracture surfaces in each borehole are presented in Appendix B.

There is a spread of impact values, both for each fracture but also between fractures. No clear correlation with AT geometry class is observed. Many fractures have impact values below the measurement limit for the selected hardness scale with measuring range,  $L_D = 80-976$ . The main reason for this is not that the fracture surfaces are too soft, but that the Leeb instrument is very sensitive to the roughness of the fracture surface in order to get an optimal impact. This is examined in more detail in Chapter 5-7 where a different hardness scale with a lower measuring range is used.

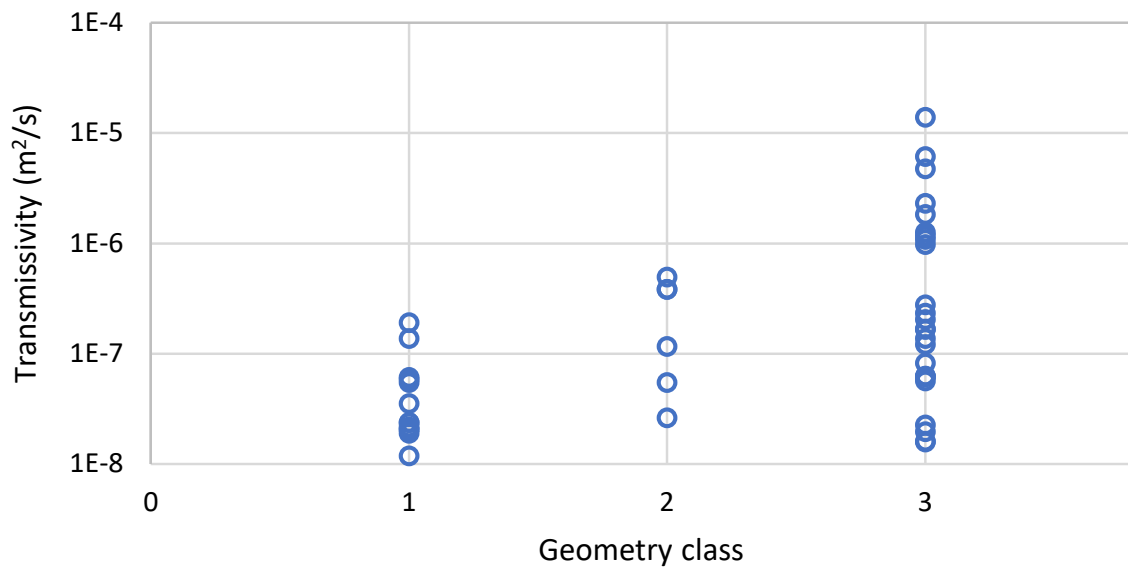
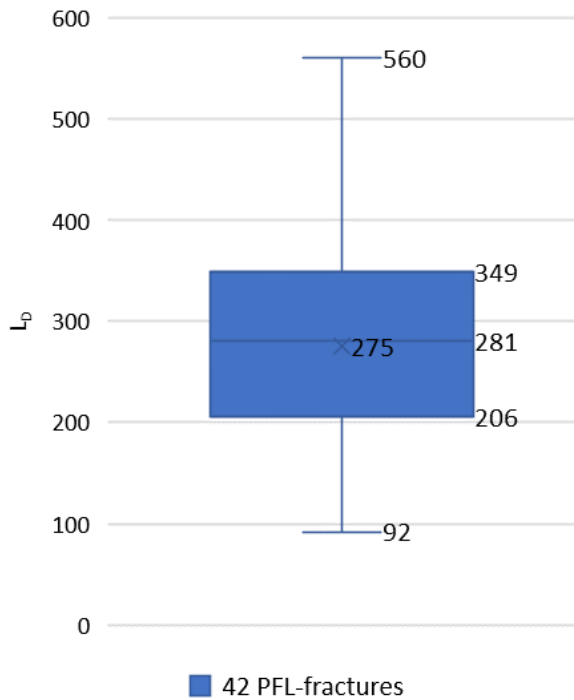


Figure 5-12. Transmissivity of the 42 tested PFL-fractures in the geometry class I-III.

**Table 5-6. Result from LHT for PFL-fractures.**

Fracture depth (m)	Average $L_D$	Transmissivity	Total number of impacts	Percentage of AML	Percentage of BML
120.900	272	$1.66 \times 10^{-7}$	47	0	57
121.897	163	$6.11 \times 10^{-8}$	40	0	18
131.270	291	$1.90 \times 10^{-8}$	22	0	5
145.553	207	$2.32 \times 10^{-7}$	47	0	55
147.925	443	$2.30 \times 10^{-6}$	22	0	9
150.867	92	$1.91 \times 10^{-7}$	24	0	92
369.430	249	$1.60 \times 10^{-8}$	38	0	47
377.827	281	$8.22 \times 10^{-8}$	48	0	58
431.509	416	$6.22 \times 10^{-8}$	21	0	10
70.806	375	$2.17 \times 10^{-8}$	20	0	5
76.018	560	$1.82 \times 10^{-6}$	20	0	0
84.494	293	$1.16 \times 10^{-7}$	19	0	5
87.904	163	$4.72 \times 10^{-6}$	24	0	17
89.612	348	$1.39 \times 10^{-5}$	23	0	13
91.914	-	$1.08 \times 10^{-6}$	21	0	100
93.803	165	$3.82 \times 10^{-7}$	62	0	42
94.999	339	$2.77 \times 10^{-7}$	24	0	17
96.424	177	$3.64 \times 10^{-7}$	30	0	33
98.322	140	$1.37 \times 10^{-7}$	44	0	18
101.421	204	$5.48 \times 10^{-8}$	48	0	25
113.018	245	$1.18 \times 10^{-8}$	42	0	14
116.841	230	$2.06 \times 10^{-8}$	26	0	23
118.624	163	$2.62 \times 10^{-8}$	55	0	64
120.876	161	$6.10 \times 10^{-8}$	29	0	24
315.306	220	$2.04 \times 10^{-7}$	22	0	0
328.076	283	$1.95 \times 10^{-8}$	23	0	9
328.723	287	$2.25 \times 10^{-8}$	23	0	13
334.430	293	$5.63 \times 10^{-8}$	20	0	0
436.362	234	$1.26 \times 10^{-6}$	32	0	28
480.296	381	$2.04 \times 10^{-8}$	29	14	14
480.724	367	$2.36 \times 10^{-8}$	28	7	14
80.205	171	$6.13 \times 10^{-6}$	28	0	32
82.264	220	$4.95 \times 10^{-7}$	26	0	27
91.856	349	$5.46 \times 10^{-8}$	27	0	26
92.374	231	$1.21 \times 10^{-7}$	32	0	41
93.320	229	$3.51 \times 10^{-8}$	34	0	44
94.967	362	$9.74 \times 10^{-7}$	23	0	9
95.587	310	$1.17 \times 10^{-6}$	23	0	13
96.289	411	$1.37 \times 10^{-7}$	22	0	0
98.333	384	$5.83 \times 10^{-8}$	23	0	4
104.356	286	$1.67 \times 10^{-7}$	27	0	26
151.028	284	$1.58 \times 10^{-8}$	27	0	26



**Figure 5-13.** Boxplot of the 42 tested PFL-fractures. Each value is the average of 20 impacts on the fracture surface where result is obtained. The box includes the middle 50 % of the fractures. The end marks lie at maximum and minimum values. The x mark gives the median value and the line in the middle is the mean value.

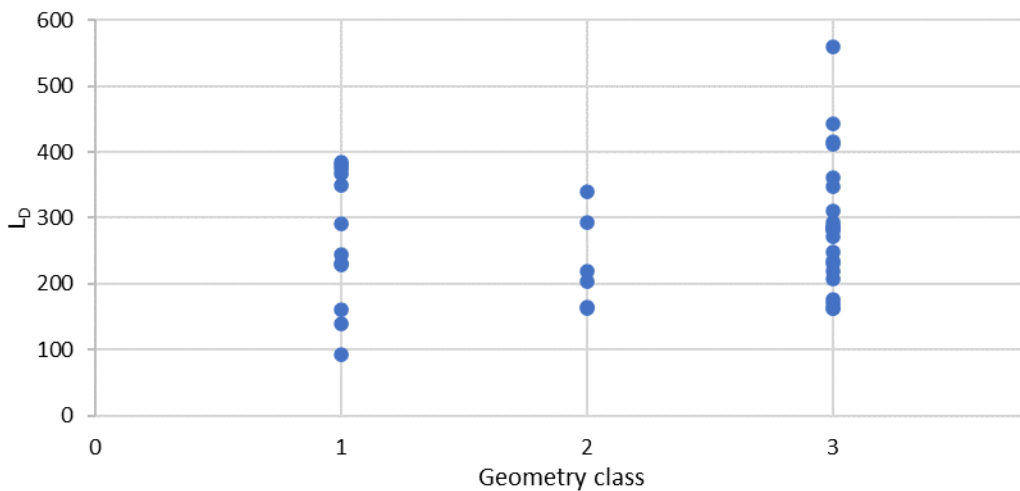


**Figure 5-14.** LD vs geometry AT- classes I-III. Classes are explained in **Table 2-2**.

## 5.4 LHT on natural Non-PFL-fracture surfaces

For comparison, surfaces from 21 Non-PFL-fractures were tested with Leeb hardness test, using the same hardness scale and setup. The result is presented in **Table 5-7** and **Figure 5-15**. As for the PFL-fractures, the tests conducted on the non-PFL did not show any impact value above measurement limit (AML) for the selected hardness scale. However, the non-PFL-fractures showed a noticeable lower percentage of measurements below the limit (BML), compared to the PFL-fractures.

**Table 5-7. Results from LHT on Non-PFL-fractures.**

Fracture depth (m)	Average $L_D$	Total number of impacts	Percentage of AML	Percentage of BML
<b>KFM01D</b>				
127.744	371	21	0	5
122.355	386	26	0	12
139.844	315	32	0	38
143.393	477	22	0	9
151.937	187	23	0	13
152.272	208	21	0	0
362.929	293	23	0	13
364.077	415	24	0	17
378.019	440	23	0	13
428.089	417	24	0	13
<b>KFM10A</b>				
116.038	170	67	0	46
121.167	272	53	0	32
123.077	234	48	0	25
149.427	279	39	0	5
183.379	313	39	0	8
<b>KFM11A</b>				
86.118	236	29	0	31
100.19	297	21	0	0
114.993	301	22	0	9
111.933	271	20	0	0
146.661	568	20	0	0
150.124	340	32	0	38

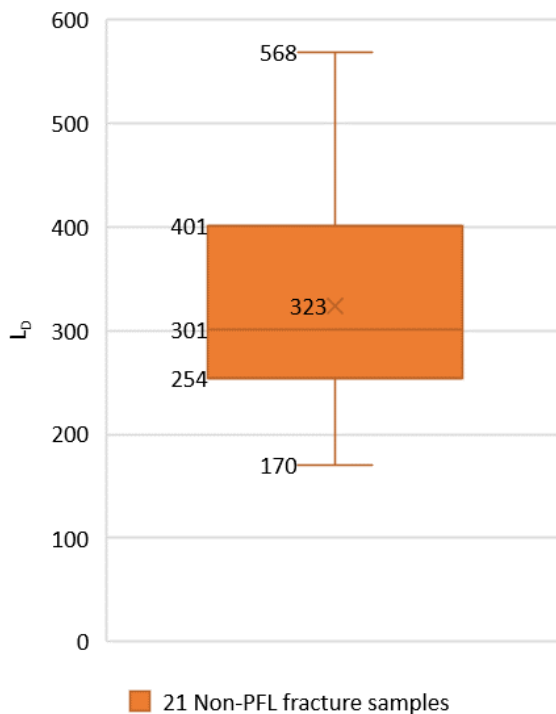


**Figure 5-15.** Box plot of LHT results for the 21 tested Non-PFL fractures surfaces.

## 5.5 Comparison of LHT on PFL-fractures and Non-PFL-fracture surfaces

A comparison of the LHT result for PFL- and Non-PFL-fractures is presented in Figure 5-16 and Figure 5-17. Although the spread is large in both groups a difference in hardness can be distinguished between the two types of fractures. On average, the LHT is about 15 % lower for the PFL-fractures compared to Non-PFL-fractures. However, considering that the LHT with the selected hardness scale resulted in more impacts below the measurement limit (BML) for the PFL-fractures, this 15 % difference underestimates the real difference.

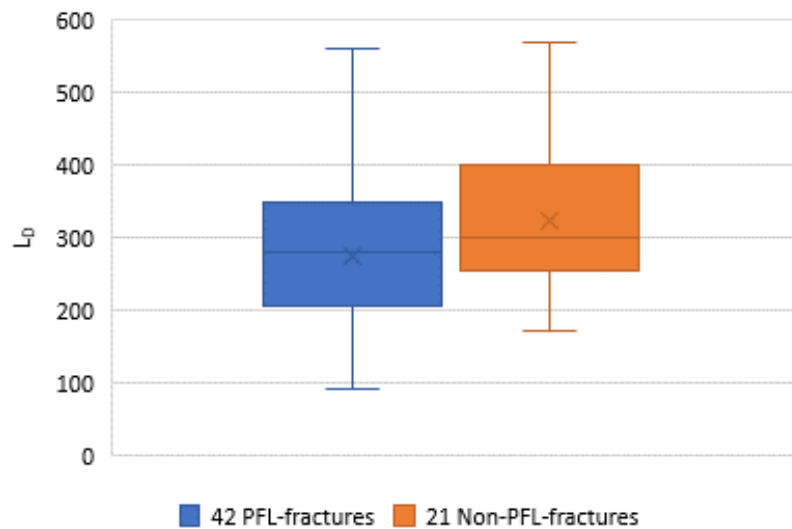


Figure 5-16. Comparison of LHT result on PFL- and Non-PFL-fractures.

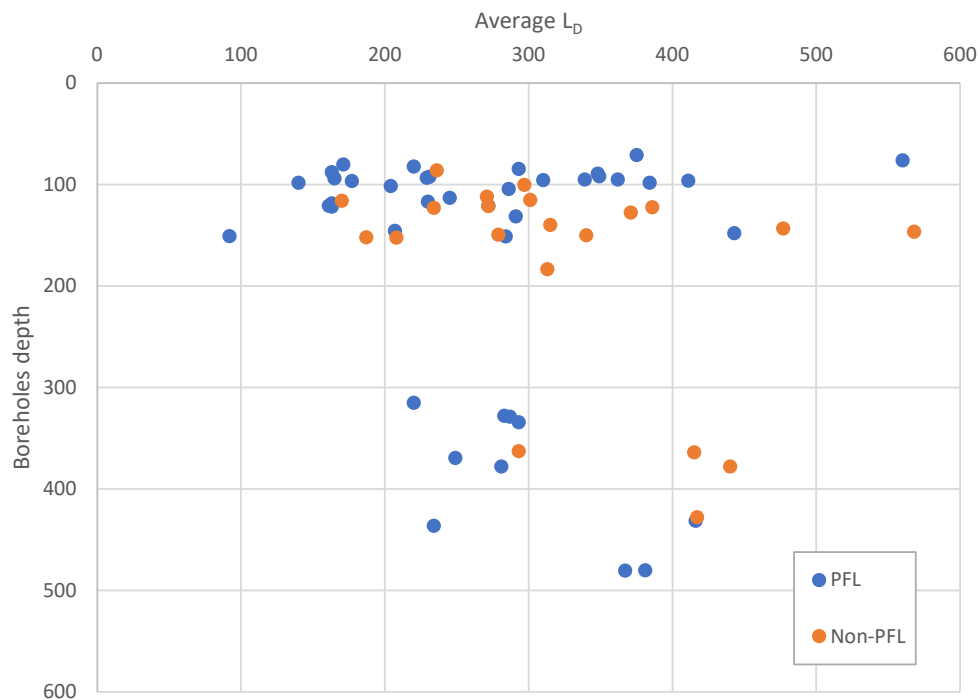
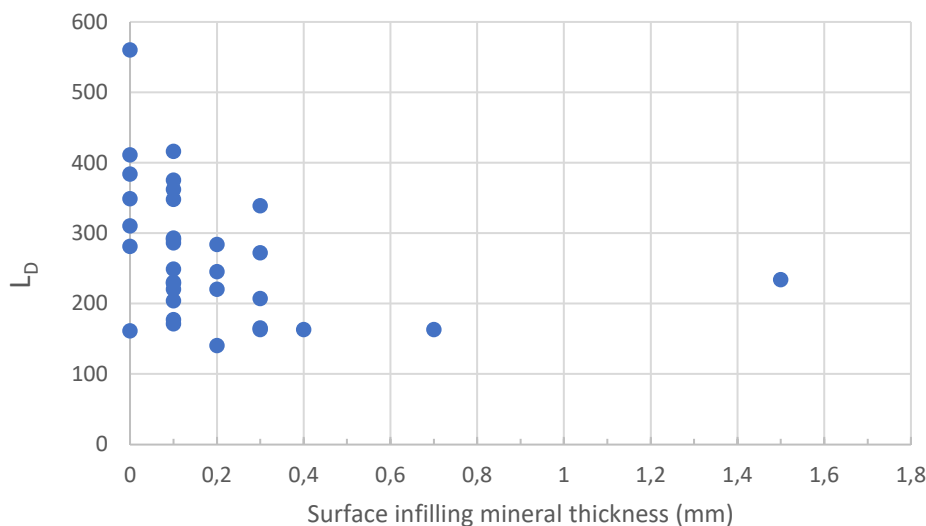


Figure 5-17. The LHT results vs the borehole depth for the tested fractures. Note that not all PFL-fractures are included in the LHT study, which explains the lack of points in the depth interval 200-300 m depth.

## 5.6 Correlation between LHT and detailed infilling mapping

A detailed mineralogical characterization was conducted in some parts of the borehole KFM01D, KFM10A and KFM11A (Eklund and Mattsson 2009). In these sections there are located some of the fractures included in the LHT study. Thus, it was possible to try to find any correlation between the amount of fracture infilling and the Leeb hardness test result. The thickness parameter is defined here as the sum of the thicknesses of the different infilling materials on the fracture side with the highest estimated thickness during the detailed mapping, which corresponds here to the LHT tested surface. The amount of infilling material is only roughly estimated from the percentage of total coverage area multiplied by the estimated thickness, which is not a very accurate number.

It can be noted from the Figure 5-18 that a slight correlation may exist, showing lower  $L_D$  for increasing infilling, however the spread is large and the number of fractures with thicker average infilling is too low for conclusive observations. It was seen in Section 3.5 that there is no main difference between the PFL fracture and the non-PFL, in terms of the type of infilling (Figure 3-8). This corresponds to the results in a previous performed study of core fracture mapping (Sandström et al. 2008). However, the study of Sandström et al. (2008) did not estimate the amount (thickness) of the infilling, only the types of minerals.



**Figure 5-18.** The LHT results on some PFL-fractures versus the estimated surface infilling thickness estimates based on data by Eklund and Mattsson (2009).

## 5.7 Complementary LHT with different hardness scales

As previously shown (Sections 5.2-5.4), the Leeb hardness test instrument can give an impact value only within a certain range of hardness, which depends on the selected hardness scale used for the measurements. In all the previous tests the hardness scale with measuring range 80–976 has been used, but since a considerable number of the impacts on fracture surfaces resulted in values “Below measurement limit”, it was decided to conduct a parallel study to see whether using a different scale would be a better choice. Among the previously tested surfaces, fourteen natural PFL-fracture surfaces with different character were selected for this comparison and tested using the hardness scale with measuring range 45–315. The result is presented in Figure 5-19.

In general, as expected, the tests using the lower scale (45–315) resulted in fewer impacts “Below measurement limit”, but also in impacts “Above measurement limit” in several cases. With one exception, the 80–976 measuring range gives higher impact values than the 45–315 scale. This indicates that the hardness scale 80–976 overestimates the real average value in those cases with a significant amount of BML impacts. Conversely, the hardness scale 45–315 underestimates the real average in the cases where there are many AML.

Looking at some examples: Sample 3 has a much higher  $L_D$  value using the hardness scale with higher range, where about 10 % of the impacts are below the measurement limit. This is in agreement with the fact that the lower hardness scale gives about 27 % of impacts above the limit and 4 % below limit. For impacts below the measurement limit one should consider that there are two possible explanations behind that result: an actually softer mineral, or a non-smooth impact point giving a sliding or crushing “softer” rebound, compared to a smooth surface with the same mineral. In this case the surface was very rough and it was judged to be the main reason for the BML.

Sample 6 is a surface that seems to have an average hardness that lies within both scales, 170 and 220 in average. These differences could be a result of the different minerals and roughness at the randomly chosen points for the impacts on the surface or even due to a possible systematic difference between scales. For sample 7 all impacts were within range in the lower scale and for this sample the results are the same for both scales.

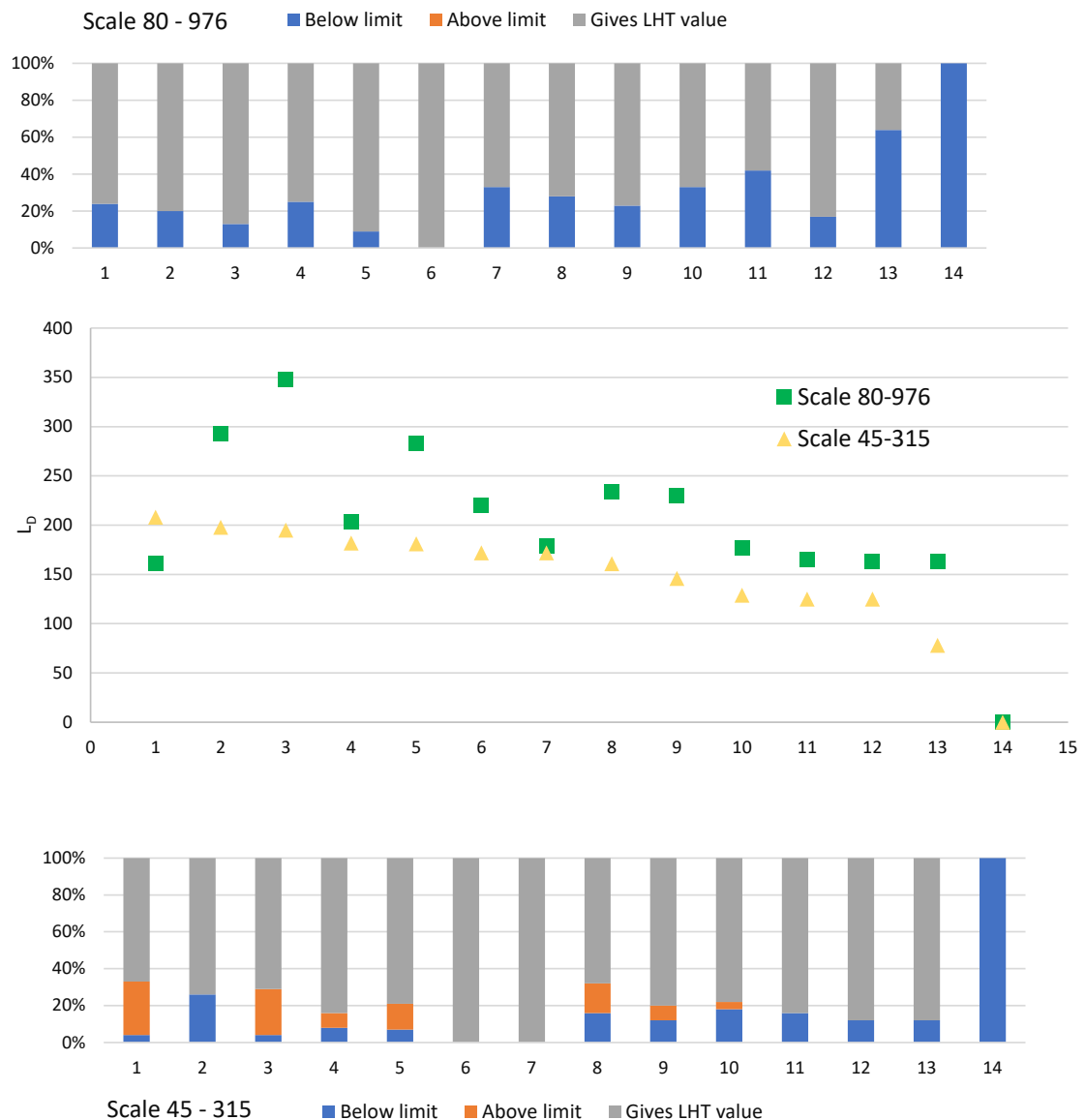


**Figure 5-19.** Results from LHT on 14 different PFL-fractures, using two different scales on the instrument. The upper and lower diagrams present the distribution of impact result for the two scales respectively. The diagram in the middle shows the average  $L_D$  value for the two cases, sorted after the estimated value using scale 45–315 from higher to lower.

An example where the lower scale probably gives a more correct average value is sample 13. For this softer sample the high scale gets many impacts below limit. The difference in calculated average  $L_D$  when using the two different scales is consequently large, while the lower scale value is probably the more correct value.

The conclusion drawn after this scale comparison is that, none of the hardness scales available in the specific model of Leeb hardness tester used in this study is suitable for all types of rock fractures, since the range of hardness is too large. It is judged that the general understanding of the PFL-fractures, based on results from using the higher scale, would not have become different using another scale. An advantage of the higher scale is that it can be used also on intact rock, although limited to the softer rock types. To use a mixture of scales is not recommended because there may be some systematic differences and complications with calibration would be added.

In the following section the Leeb hardness test, and the evaluation of its applicability after this pilot study will be discussed.

## 5.8 Discussion on Leeb hardness test (LHT) device and method

The Leeb hardness test (LHT) was introduced and used for the first time by SKB on rock and fracture samples from the Forsmark site within this study. The objective was to evaluate the method, the specific Leeb device used and to assess its applicability for further use within the Forsmark site investigations before, during and after the construction of the final storage of spent nuclear fuel.

Several advantages and disadvantages were found during the pilot study regarding the method and the particular TIME model of Leeb hardness tester used. Pros and cons are summarized in the following points:

- The instrument is affordable.
- It is possible to conduct many tests in a short time and requires no preparation.
- The functionality of the instrument is very good on smooth surfaces such as the cut cross-sections and quite good on cylindrical drill core surfaces.
- The particular Leeb device used in this study lacks of a hardness scale with a suitable measuring range to avoid impact values below and above measurement limit for most of the rock types in the Forsmark site.
- Using the Leeb instrument on fracture surfaces clearly captures their differences but it also entails several difficulties;
  - The fracture roughness makes difficult getting an optimal impact resulting in a hardness value that reflects the mineral composition of the surface. Furthermore, the roughness results in a wide spread of the hardness values and also in a considerable number of impacts below the measurement limit even if the surface is hard.
  - There is no hardness scale available in the tested Leeb hardness instrument that covers all types of fracture mineral fillings, from *no detectable mineral* to *clay mineral*.
- An interesting observation is that in some occasions the tested Leeb hardness instrument began to malfunction after conducting a few tests. The trigger button stopped working after about 5 tests and the instrument needed to rest for a day or so before it was functional again. No error message was shown on the display.

## 6 Summarizing conclusions and recommendations

### 6.1 Comparison between PFL-fractures and Non-PFL-fractures

In previous chapters the characteristics of fractures, that have been correlated to borehole sections with transmissivity higher than ca  $10^{-9}$  m<sup>2</sup>/s, inferred with the Posiva Flow Log (called PFL-fractures), have been compared to other open fractures (called non-PFL-fractures) in different ways. The following points summarize these findings:

- PFL-fractures and Non-PFL-fractures have similar distribution of parameters for the single surface case (stepped/undulating/irregular/planar and rough/smooth/slickensided).
- PFL-fractures and Non-PFL-fractures have similar distribution of the dominant type of infilling mineral ("Mineral 1" according to the Boremap mapping system).
- PFL-fractures are expected to have slightly more amounts of infilling minerals, but a large spread in mineral occurrence exists.
- The measurements with the Leeb hardness test (LHT) showed that the surfaces of PFL-fractures are softer than the Non-PFL-fractures. The spread in LHT-values is large in the two groups, both over each single fracture surface and between fracture samples. On average the LHT is approximately 15 % lower for the PFL-fractures compared to Non-PFL-fractures. However, considering that the used LHT hardness scale resulted in more values below measurement limit for the PFL-fractures, this 15 % difference is probably underestimating the real difference to a degree that has not been determined. Additional tests are needed to give more reliable results.
- About 65 % of PFL fractures have been assigned the geometrical classification of a single structural feature (Class I-III).
- About 23 % have been classified with geometry Class IV, which corresponds to 2-3 fractures close to each other, often subparallel.
- About 12 % of the PFL-anomalies are located at very complex structural features with many fractures (Class V-VII), (some of these corresponds to mapped crush).
- Despite of the limited investigations made, the PFL-fractures with higher flow seem to have less mated fractures surfaces compared to fractures with lower flow.
- Most PFL-fractures seem to have fracture surfaces that are not in contact at the borehole intersection.

## 6.2 Recommendations and concluding remarks

Based on the results from this study the following conclusions have been drawn with respect to the approaches for the estimation of mechanical properties for intact rock surfaces and fractures surfaces of different kinds:

The PFL-fractures are expected to have a hydro-mechanical stress dependent behaviour different than the behaviour of the Non-PFL fractures.

The Leeb hardness test (LHT) with the particular Leeb device used in this study is not a perfectly accurate method for quantifying the stiffness of natural fractures or even the hardness of the separate fracture surfaces. However, the LHT is able to detect qualitatively the softer surface character which prevails for PFL-fractures, on the average, compared to Non-PFL-fractures.

LHT is recommended in situations where very fast and low-cost qualitative estimates are of interest and when the characterization is not possible with other means. For example, if an unknown rock type or variations in rock types occur, LHT results from saw cuts of the drill core may give a first indication that the occurrence is outside the previously expected one, and help in the selection of samples for laboratory testing.

In future investigations, the hardness scale limitation of the particular Leeb instrument employed in this study may be overcome by using a different device that includes a broader measuring range with lower and higher hardness limits, suitable for the dominating strong rock types and fracture surfaces in Forsmark. This instrument could be a different model or modified Leeb hardness tester, or even the Schmidt hammer.

The fracture matedness is an important factor for the flow properties of single fractures. Therefore, the development of measurement techniques for determining fracture matedness may be a potential area to improve the aperture spatial distribution models. This in turn would be useful in the estimation of fracture hydro-mechanical properties for the water bearing fractures in the Forsmark site.

## References

SKB's (Svensk Kärnbränslehantering AB) publications can be found at [www.skb.com/publications](http://www.skb.com/publications).

- Barton N, 2002.** Some new Q-value correlations to assist in site characterization and tunnel design. *International Journal of Rock Mechanics and Mining Science*, 39/2, 185-216.
- Barton N, Choubey V, 1977.** The Shear Strength of Rock Joints in Theory and Practise. *Rock Mechanics* 10, 1-54.
- Claesson Liljedahl L, Munier R, Sandström B, Drake H, Tullborg E-L, 2011.** Assessment of fractures classified as non-mineralized in the Sicada database. SKB R-11-02, Svensk Kärnbränslehantering AB.
- Corkum A G, Asiri Y, El Naggat H, Kinakin D, 2018.** The Leeb hardness test for rock: An updated methodology and UCS correlation. *Rock Mechanics and Rock Engineering* 51, 665-675.
- Eklund S, Mattsson K-J, 2009.** Quantitative mapping of fracture minerals in Forsmark. Forsmark site investigation. SKB P-08-47, Svensk Kärnbränslehantering AB.
- Follin S, 2008.** Bedrock hydrogeology Forsmark. Site descriptive modelling, SDM-Site Forsmark. SKB R-08-95, Svensk Kärnbränslehantering AB.
- Forsman I, Zetterlund M, Rhén I, 2004.** Correlation of Posiva flow log anomalies to core mapped features in Forsmark (KFM01A to KFM05A). SKB R-04-77, Svensk Kärnbränslehantering AB.
- Forssman I, Zetterlund M, Forsmark T, Rhén I, 2006.** Correlation of Posiva flow log anomalies to core mapped features in KFM06A and KFM07A. Forsmark site investigation. SKB P-06-56, Svensk Kärnbränslehantering AB.
- Forssman I, Forsmark T, Rhén I, 2008.** Correlation of Posiva flow log anomalies to core mapped features in KFM02B, KFM08D and KFM11A. Forsmark site investigation. SKB P-07-128, Svensk Kärnbränslehantering AB.
- Glamheden R, Fredriksson A, Röshoff K, Karlsson J, Hakami H, Christiansson R, 2007.** Rock mechanics Forsmark. Site descriptive modelling Forsmark stage 2.2. SKB R-07-31, Svensk Kärnbränslehantering AB.
- Hakami E, 1992.** Joint aperture measurements – An experimental technique. *Proc. of the Conf. on Fractured and Jointed Rock Masses, Lake Tahoe, California, USA, 1992*, p 453-456.
- Hakami E, Mas Ivars D, Darcel C, 2022.** Methodology for rock mechanics modelling of the Forsmark site. SKB R-20-13, Svensk Kärnbränslehantering AB.
- Hanquist C, Jacobsson L, Davidsson S, 2023.** Laboratory tests in borehole KFM01A, KFM08A, KFM11A, KFR102A and KFR104. Uniaxial compression and indirect tensile strength tests of intact rock. SKB P-23-05. Svensk Kärnbränslehantering AB.
- Jeans B, 2021.** Leeb Hardness Test for rock joint wall compressive strength evaluation [Master of Applied Science (MAsc), Dalhousie University]. Halifax, Nova Scotia.
- Ringgard J, 2007.** Mapping of borehole breakouts. Processing of acoustical televiwerdata from KFM01A, KFM01B, KFM02A, KFM03A, KFM03B, KFM04A, KFM05A, KFM06A and KFM07C. SKB P-07-07, Svensk Kärnbränslehantering AB.
- Sandström B, Tullborg E-L, 2011.** Fracture mineralogy and geochemistry of borehole sections sampled for groundwater chemistry and Eh. Results from boreholes KFR01, KFR08, KFR10, KFR19, KFR7A and KFR105. Site investigation SFR. SKB P-11-01, Svensk Kärnbränslehantering AB.

**Sandström B, Tullborg E-L, Smellie J, MacKenzie A B, Suksi J, 2008.** Fracture mineralogy of the Forsmark site. SDM Forsmark. SKB R-08-102, Svensk Kärnbränslehantering AB.

**Selroos J-O, Mas Ivars D, Munier R, Hartley L, Libby S, Davy P, Darcel C, Trincherio P, 2022.** Methodology for discrete fracture network modelling of the Forsmark site. Part 1 – concepts, data and interpretation methods. SKB R-20-11, Svensk Kärnbränslehantering AB.

**Teurneau B, Forsmark T, Forssman I, Rhén I, Zinn E, 2008.** Correlation of Posiva Flow Log anomalies to core mapped features in KFM01D, KFM07C, KFM08A, KFM08C and KFM10A. Forsmark site investigation. SKB P-07-127, Svensk Kärnbränslehantering AB.

## Appendix A – Acoustic televiewer image files with geometry classification of PFL anomalies

Each borehole at Forsmark that has both acoustic televiewer and the Posiva Flow logging performed is included in this study (see also Table 2-1). The geometry classification performed is documented in WellCAD-files (.WCL) for each borehole with the following filenames:

KFM01A.WCL  
KFM01D\_84-379.WCL  
KFM01D\_374-796.WCL  
KFM02A\_0-299.WCL  
KFM02B\_69-405.WCL  
KFM02B\_400-570.WCL  
KFM04A\_108-1000.WCL  
KFM05A\_104-1000.WCL  
KFM08C\_0-950.WCL  
KFM08D\_49-928.WCL  
KFM10A\_0-496.WCL  
KFM11A\_59-623.WCL

To study the files the full licence program WellCAD, or the freeware WellCAD Reader, is needed.

By using a realistic depth length scale the shape of the fractures in the logs can be studied.

As an example, a short section of the file from borehole KFM05A is given in the following three pages (in this example case the depth scale is still too compressed to give the correct shape of structures, but it shows what kind of information is given in the WellCAD files).

At the depth of each fracture/structure correlated with a PFL anomaly the measured transmissivity is given and the geometry class determined, as explained in Chapter 2.

Borehole ID: KFM05A

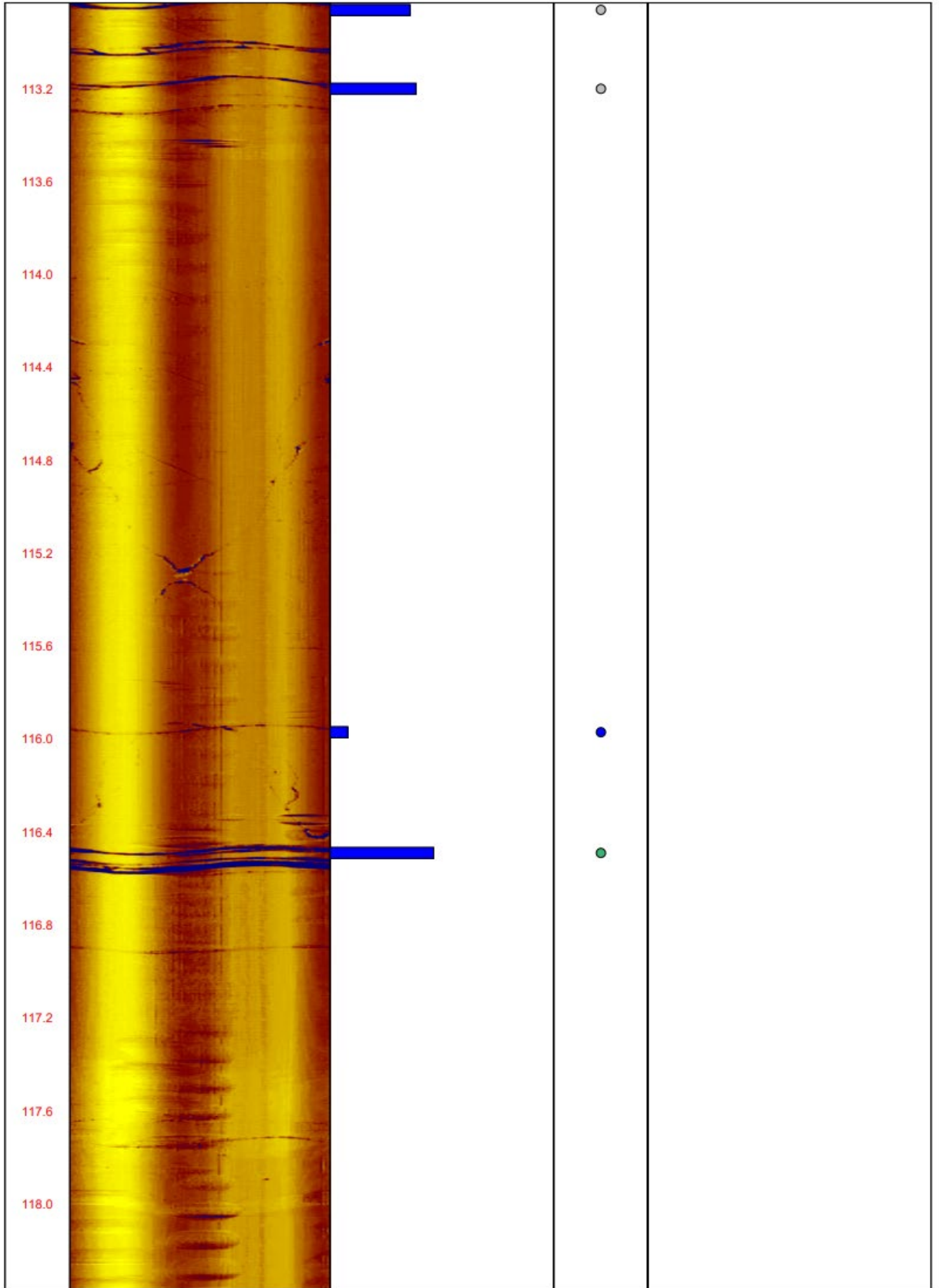
Borehole length (m): 1000

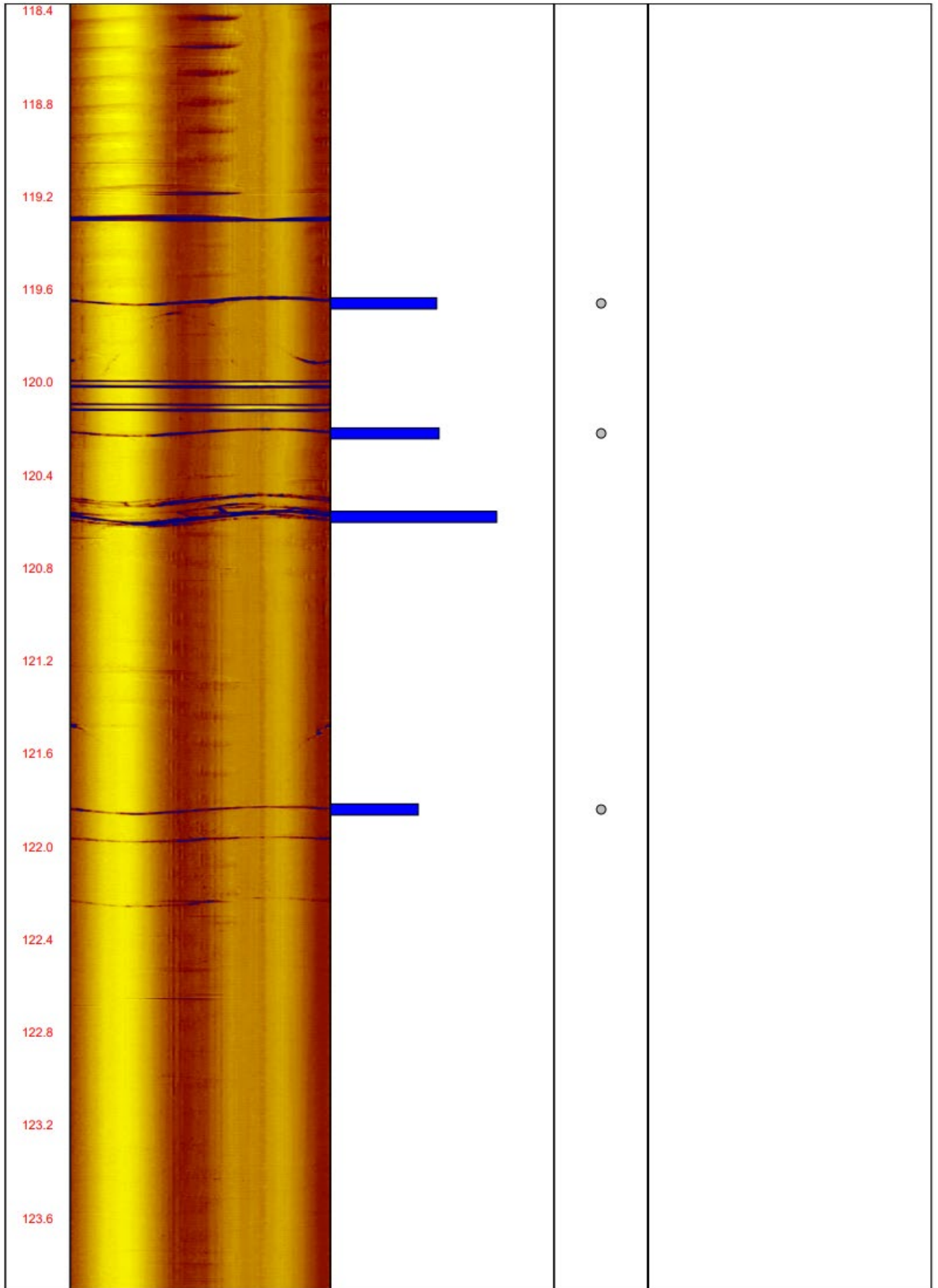
Borehole orientation (°): 081/-60



- Class I ●
- Class II ●
- Class III ●
- Class IV ●
- Class V ●
- Class VI ●
- Class VII ●

Adjusted 1m:20m	Acoustic Televiewer					Transmissivity (m <sup>2</sup> /s)		PFL geometry class	Comment		
	0°	90°	180°	270°	0°	2e-10	2e-05				
109.2											
109.6											
110.0										End of casing	
110.4											
110.8											
111.2											
111.6										●	
112.0											
112.4										●	
112.8											





## Appendix B – Photographs of studied PFL-fracture surfaces

KFM01D, 120.901 m



KFM01D, 121.897 m



KFM01D, 131.270 m



KFM01D, 145.553 m



KFM01D, 147.935 m



KFM01D, 369.430 m



KFM01D, 377.827 m



KFM01D, 431.509 m



KFM10A, 70.806 m



KFM10A, 76.018 m



KFM10A, 84.494 m



KFM10A, 87.904 m



KFM10A, 89.612 m



KFM10A, 91.920 m



KFM10A, 93.803 m



KFM10A, 94.999 m



KFM10A, 96.424 m



KFM10A, 98.322 m



KFM10A, 101.421 m



KFM10A, 113.018 m



KFM10A, 116.841 m



KFM10A, 118.624 m



KFM10A, 120.876 m



KFM10A, 315.306 m



KFM10A, 328.076 m



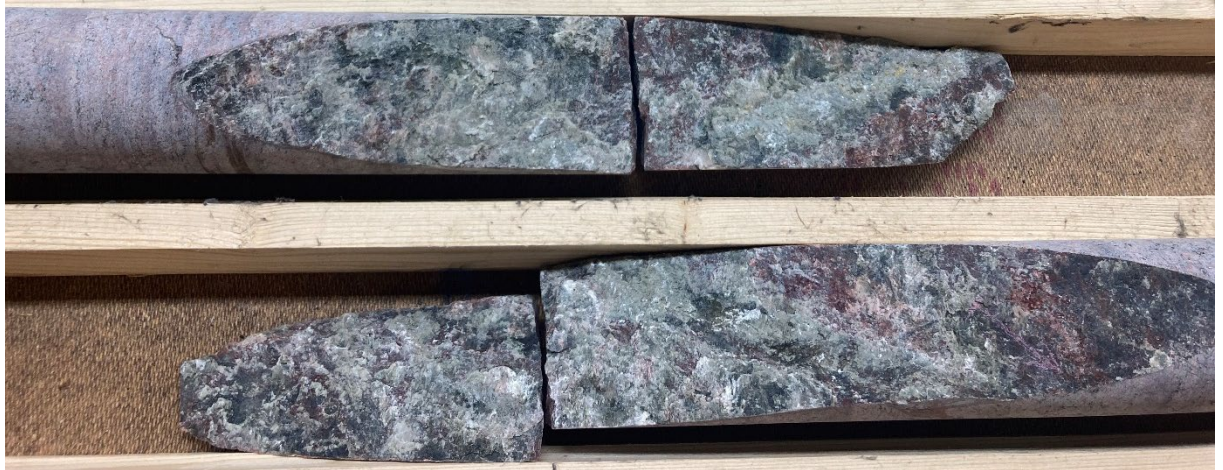
KFM10A, 328.723 m



KFM10A, 334.430 m



KFM10A, 436.362 m



KFM10A, 437.869 m



KFM10A, 480.296 m



KFM10A, 480.724 m



KFM11A, 80.205 m



KFM11A, 80.264 m



KFM11A, 91.856 m



KFM11A, 92.374 m



KFM11A, 93.320 m



KFM11A, 94.967 m



KFM11A, 95.587 m



KFM11A, 96.289 m



KFM11A, 98.333 m



KFM11A, 151.028 m

